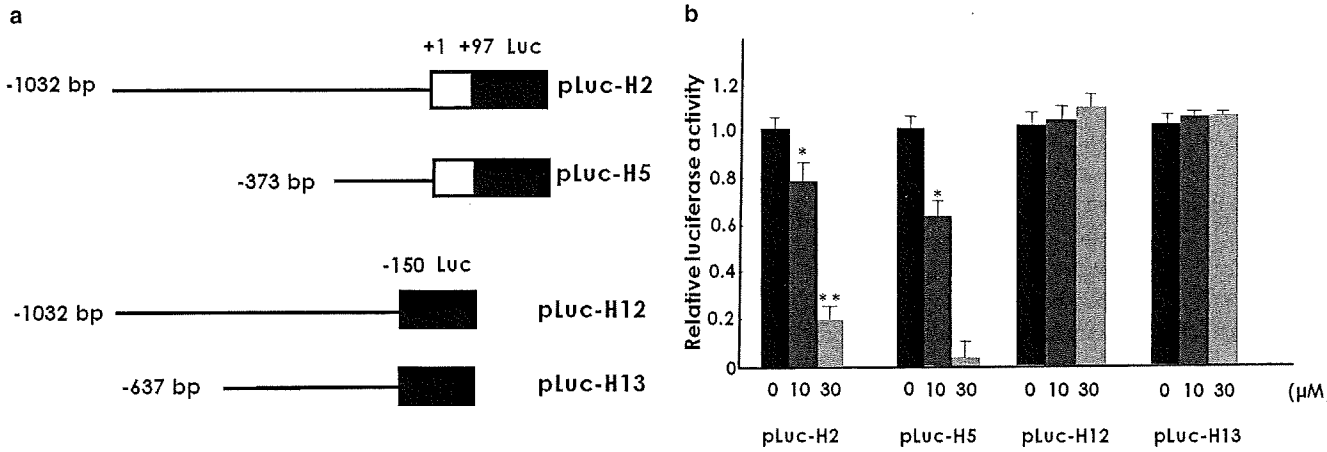

Fig. 7. Possible action site of vitamin K_2 in the promoter of the HDGF gene. **a** The construct of the luciferase-reporter assay plasmids for the HDGF promoter region. **b** SK-Hep-1 cell was transfected with 1 μg each promoter vector (pLuc-H2, -H5, -H12, -H13). After incubation with the indicated concentrations (μM) of vitamin K_2 for 24 h, the cells were harvested, and the relative luciferase activities were measured. Data are shown as mean ± SE of three independent experiments. $^*P < 0.05$; $^{**}P < 0.01$ vs. control

pression of HDGF is one of the pathways to inhibit cell growth by vitamin K_2 treatment, through its interaction with the promoter region of the HDGF gene.

Discussion

The inhibitory mechanisms of vitamin K_2 in cancer cell proliferation have not yet been clarified. Some possible pathways of vitamin K_2 action have been reported, specifically protein kinase A activation, the induction of cell-cycle regulatory proteins, and the suppression of the cyclin-dependent kinases.[26–28] Another pathway has been reported to suppress the cyclin D1 expression through the inhibition of nuclear factor (NF) kappa B activation.[29] Recently, vitamin K_2 is reported to inhibit the phosphorylation of the retinoid X receptor (RXR) alpha protein, which is a critical factor for hepatocarcinogenesis.[30] We previously reported that p21 induction is a significantly important pathway for the growth inhibitory action of vitamin K_2 by the use of HepG2 cells.[28] However, vitamin K_2 suppressed the growth of the HuH-7 cells more strongly than the HepG2 cells, although the HuH-7 cells are deficient in the p21WAF1/CIP1 protein. Therefore, other mechanisms for the vitamin K_2 growth inhibition remained to be clarified.

In the present study, vitamin K_2 significantly suppressed HDGF mRNA and protein expression in HCC cells. Few data have been reported about the inhibition of the expression of growth factor and/or growth factor receptor genes in HCC cells. Acyclic retinoid suppressed fibroblast growth factor (FGF) receptor 3 gene expression in an HCC cell line.[31] Therefore the downregulation of HDGF by vitamin K_2 should play an important role in the suppression of HCC cell growth by vitamin K_2.

HDGF is one of the critical growth factors that play important roles in the proliferation of HCC cells. Enhanced expression of HDGF showed malignant potential of tumor cells and a poorer prognosis in patients with HCC as well as gastric cancer, lung cancer, and pancreatic cancer.[12,13,15,16,18,19,32] Downregulation of HDGF may induce cancer growth inhibition and improve the prognosis for cancer patients. Indeed, the downregulation of HDGF by either antisense oligonucleotides or antisense viral treatment and gene silencing by siRNA inhibit the cell growth both in vitro and in vivo.[8,14,17] In the present study, the knock-down expression of HDGF by shRNA partially suppressed the proliferation of SK-Hep-1 cells. Thus, HDGF is apparently one of the growth factors involved in the proliferation of HCC cells. On the other hand, other growth factors, including hepatocyte growth factor (HGF), FGF, epidermal growth factor (EGF), HB-EGF, and transforming growth factor-alpha (TGF-α), should be related to the proliferation of HCC; however, until now, no evidence has been reported that vitamin K_2 suppressed these growth factors and their receptors. In the present study, we showed a significant suppression of the HDGF gene expression by vitamin K_2. This is the first report that vitamin K_2 regulates the expression of growth factor genes. The regulation of the gene expression of one growth factor, HDGF, by vitamin K_2 suggests to us an important approach to investigate the mechanisms of vitamin K action.

By a luciferase assay using the promoter region of HDGF, vitamin K_2 significantly downregulated the

HDGF expression. Vitamin K_2 must act directly or indirectly on the promoter region of HDGF and regulate the expression of HDGF. Recently, vitamin K_2 suppressed cyclin D1 expression through inhibition of nuclear factor (NF)-kappaB activation with inhibition of phosphorylation and degradation of I-kappaB alpha and I-kappaB kinase activity.[29] In the promoter region of −150 to 0 in the HDGF gene, no NF-kappaB binding site could be detected. Other transcriptional factors, including cAMP response element-binding protein (CREB), upstream transcription factor (USF), and activating enhancer-binding protein (AP)-2, are reported to mediate the vitamin K_2 effects; however, their binding motifs are absent in this promoter region of HDGF (−1 to −150). Therefore, another pathway should be critical for the suppression of the HDGF gene expression by vitamin K_2. It remains to be clarified whether vitamin K_2 directly reacts to the DNA sequence or indirectly via other factors, including transcriptional regulatory factors or binding cofactors. Vitamin K_2 may possibly downregulate some of other growth factor genes, too. It is very important to clarify the mechanism whereby vitamin K_2 reacts on and suppresses the promoter activity of the HDGF gene. These findings suggested that the regulation of growth factor gene expression is one of the crucial mechanisms of the vitamin K_2-induced cell growth inhibition.

In conclusion, the downregulation of the HDGF expression in the promoter region is one of the growth inhibitory mechanisms of vitamin K_2. To elucidate the suppressive mechanism of the HDGF promoter region by vitamin K_2 will possibly lead to the development of a novel growth inhibitory mechanism, thus resulting in a new drug design.

Acknowledgments. This study was supported by a Grant-in-aid of Hyogo Science and Technology Association, Grant-in-aid for researchers, Hyogo College of Medicine, and Health and Labour Sciences Research Grants (Research on Hepatitis).

References

1. Nakamura H, Kambe H, Egawa T, Kimura Y, Ito H, Hayashi E, et al. Partial purification and characterization of hepatoma-derived growth factor. Clin Chim Acta 1989;183:273–84.
2. Nakamura H, Izumoto Y, Kambe H, Kuroda T, Mori T, Kawamura K, et al. Molecular cloning of complementary DNA for a novel human hepatoma-derived growth factor. J Biol Chem 1994;269: 25143–9.
3. Kishima Y, Yamamoto H, Izumoto Y, Yoshida K, Enomoto H, Yamamoto M, et al. Hepatoma-derived growth factor stimulates cell growth after translocation to the nucleus by nuclear localization signals. J Biol Chem 2002;277:10315–22.
4. Everett AD, Stoops T, McNamara CA. Nuclear targeting is required for hepatoma-derived growth factor-stimulated mitogenesis in vascular smooth muscle cells. J Biol Chem 2001;276: 37564–8.
5. Okuda Y, Nakamura H, Yoshida K, Enomoto H, Uyama H, Hirotani T, et al. Hepatoma-derived growth factor induces tumorigenesis in vivo through both direct angiogenic activity and induction of vascular endothelial growth factor. Cancer Sci 2003;94:1034–1041.
6. Everett AD, Narron JV, Stoops T, Nakamura H, Tucker A. Hepatoma-derived growth factor is a pulmonary endothelial cell-expressed angiogenic factor. Am J Physiol Lung Cell Mol Physiol 2004;286:L1194–201.
7. Oliver JA, Al-Awqati Q. An endothelial growth factor involved in rat renal development. J Clin Invest 1998;102:1208–19.
8. Enomoto H, Yoshida K, Kishima Y, Kinoshita T, Yamamoto M, Everett AD, et al. Hepatoma-derived growth factor is highly expressed in developing liver and promotes fetal hepatocyte proliferation. Hepatology 2002;36:1519–27.
9. Everett AD, Lobe DR, Matsumura ME, Nakamura H, McNamara CA. Hepatoma-derived growth factor stimulates smooth muscle cell growth and is expressed in vascular development. J Clin Invest 2000;105:567–75.
10. Yoshida K, Nakamura H, Okuda Y, Enomoto H, Kishima Y, Uyama H, et al. Expression of hepatoma-derived growth factor in hepatocarcinogenesis. J Gastroenterol Hepatol 2003;18:1293–301.
11. Huang JS, Chao CC, Su TL, Yeh SH, Chen DS, Chen CT, et al. Diverse cellular transformation capability of overexpressed genes in human hepatocellular carcinoma. Biochem Biophys Res Commun 2004;315:950–8.
12. Iwasaki T, Nakagawa K, Nakamura H, Takada T, Matsui K, Kawahara K. Hepatoma-derived growth factor as a prognostic marker in completely resected non-small-cell lung cancer. Oncol Rep 2005;13:1075–80.
13. Uyama H, Tomita Y, Nakamura H, Nakamori S, Zhang B, Hoshida Y, et al. Hepatoma-derived growth factor is a novel prognostic factor for patients with pancreatic cancer. Clin Cancer Res 2006;12:6043–8.
14. Zhang J, Ren H, Yuan P, Lang W, Zhang L, Mao L. Down-regulation of hepatoma-derived growth factor inhibits anchorage-independent growth and invasion of non-small cell lung cancer cells. Cancer Res 2006;66:18–23.
15. Yamamoto S, Tomita Y, Hoshida Y, Takiguchi S, Fujiwara Y, Yasuda T, et al. Expression of hepatoma-derived growth factor is correlated with lymph node metastasis and prognosis of gastric carcinoma. Clin Cancer Res 2006;12:117–22.
16. Yamamoto S, Tomita Y, Hoshida Y, Morii E, Yasuda T, Doki Y, et al. Expression level of hepatoma-derived growth factor correlates with tumor recurrence of esophageal carcinoma. Ann Surg Oncol 2007;14:2141–9.
17. Kishima Y, Yoshida K, Enomoto H, Yamamoto M, Kuroda T, Okuda Y, et al. Antisense oligonucleotides of hepatoma-derived growth factor (HDGF) suppress the proliferation of hepatoma cells. Hepatogastroenterology 2002;49:1639–44.
18. Yoshida K, Tomita T, Okuda Y, Yamamoto S, Enomoto H, Uyama H, et al. Hepatoma-derived growth factor is a novel prognostic factor for hepatocellular carcinoma. Ann Surg Oncol 2006;13:159–67.
19. Hu TH, Huang CC, Liu LF, Lin SY, Chang HW, Changchien CS, et al. Expression of hepatoma-derived growth factor in hepatocellular carcinoma. Cancer (Phila) 2003;98:1444–56.
20. Chlebowski RT, Akman SA, Block JB. Vitamin K in the treatment of cancer. Cancer Treat Rev 1985;12(1):49–63.
21. Wang Z, Wang M, Finn F, Carr BI. The growth inhibitory effects of vitamins K and their actions on gene expression. Hepatology 1995;22:876–82.
22. Hitomi M, Nonomura T, Yokoyama F, Yoshiji H, Ogawa M, Nakai S, et al. In vitro and in vivo antitumor effects of vitamin K5 on hepatocellular carcinoma. Int J Oncol 2005;26:1337–44.
23. Hitomi M, Yokoyama F, Kita Y, Nonomura T, Masaki T, Yoshiji H, et al. Antitumor effects of vitamins K_1, K_2 and K_3 on hepatocellular carcinoma in vitro and in vivo. Int J Oncol 2005;26:713–20.

24. Habu D, Shiomi S, Tamori A, Takeda T, Tanaka T, Kubo S, et al. Role of vitamin K_2 in the development of hepatocellular carcinoma in women with viral cirrhosis of the liver. JAMA 2004; 292:358–61.
25. Mizuta T, Ozaki I, Eguchi Y, Yasutake T, Kawazoe S, Fujimoto K, et al. The effect of menatetrenone, a vitamin K_2 analog, on disease recurrence and survival in patients with hepatocellular carcinoma after curative treatment: a pilot study. Cancer (Phila) 2006;106:867–72.
26. Markovits J, Wang Z, Carr BI, Sun TP, Mintz P, Le Bret M, et al. Differential effects of two growth inhibitory K vitamin analogs on cell cycle regulating proteins in human hepatoma cells. Life Sci 2003;72:2769–84.
27. Otsuka M, Kato N, Shao RX, Hoshida Y, Ijichi H, Koike Y, et al. Vitamin K_2 inhibits the growth and invasiveness of hepatocellular carcinoma cells via protein kinase A activation. Hepatology 2004;40:243–51.
28. Liu W, Nakamura H, Yamamoto T, Ikeda N, Saito M, Ohno M, et al. Vitamin K_2 inhibits the proliferation of HepG2 cells by up-regulating the transcription of p21 gene. Hepatol Res 2007;37: 360–5.
29. Ozaki I, Zhang H, Mizuta T, Ide Y, Eguchi Y, Yasutake T, et al. Menatetrenone, a vitamin K_2 analogue, inhibits hepatocellular carcinoma cell growth by suppressing cyclin D1 expression through inhibition of nuclear factor kappaB activation. Clin Cancer Res 2007;13:2236–45.
30. Kanamori T, Shimizu M, Okuno M, Matsushima-Nishiwaki R, Tsurumi H, Kojima S, et al. Synergistic growth inhibition by acyclic retinoid and vitamin K_2 in human hepatocellular carcinoma cells. Cancer Sci 2007;98:431–7.
31. Shao RX, Otsuka M, Kato N, Taniguchi H, Hoshida Y, Moriyama M, et al. Acyclic retinoid inhibits human hepatoma cell growth by suppressing fibroblast growth factor-mediated signaling pathways. Gastroenterology 2005;128:228–31.
32. Ren H, Tang X, Lee JJ, Feng L, Everett AD, Hong WK, et al. Expression of hepatoma-derived growth factor is a strong prognostic predictor for patients with early-stage non-small cell lung cancer. J Clin Oncol 2004;22:3230–7.

＜短　報＞

Sonazoid造影超音波による新しい肝癌悪性度分類法の試み

田中　弘教[1)2)]　飯島　尋子[1)2)*]　齋藤　正紀[2)]　會澤　信弘[2)]　坂井　良行[2)]
吉川　昌平[2)]　山本　晃久[2)]　榎本　平之[2)]　岩田　恵典[2)]　康　典利[2)]
今西　宏安[2)]　下村　壯治[2)]　中村　秀次[2)]　廣田　誠一[3)]　辻村　亨[4)]
藤元　治朗[5)]　西口　修平[2)]

緒言：肝細胞癌（HCC）の悪性度評価は組織学的に行われる．一方，動注CTによる血流評価はHCCの組織学的悪性度と生物学的悪性度の予知に有用である[1)]．また結節の悪性度が増すほど異常動脈の増加がみられるなど[2)3)]，HCCの悪性度と血流には密接な関係がある．さらに悪性度の進行したHCCではKupffer細胞数が減少することも報告されている[4)]．Sonazoid®（第一三共）を用いた造影超音波は，低侵襲かつリアルタイムに血流を評価でき，さらにMicro flow imaging（MFI）などのMaximum Intensity Projection（MIP）画像を用いることで腫瘍内の微細な血管構造を描出できる．そこで今回我々はこのMIPを用いた腫瘍血管の微細脈管構築のパターンにKupffer細胞の多寡を反映するソナゾイドのKupffer相を組み合わせ，悪性度の評価を試みた．

対象および方法：2007年1月～2008年11月までに当センターでSonazoidによる造影超音波を施行した肝結節性病変597症例902結節のうち，MFIなどのMIP画像と切除または針生検により組織所見と対比しえたHCC 42結節を対象とした．装置は東芝Aplirio XG・XV，Aloka α10，Siemens Sequoia，Philips iU22を使用した．造影方法に関しては，Sonazoid 0.0075 ml/kgをbolus投与し，10-15fps，音圧2-3%で撮像し，動脈優位相（約30秒以内）と門脈優位相（2-3分後），Kupffer相（約20分後）について検討した．MIPの撮像は，主に門脈優位相を判定した後に造影剤を再注入して行った．分類方法は動脈優位相では周囲肝実質より血流の増加が見られるものをhyper，同等をiso，低下をhypoとした．門脈優位相も同様にiso，hypo，Kupffer相はhyper，iso，hypoに分類し2名以上の肝臓および超音波専門医の目視により検討した．さらにMIP所見により腫瘍内の血管構築を，微細均一な脈管のみの“Fine”，腫瘍血管を認識できる“Vascular”，太い腫瘍血管を含み不規則な形態を呈する“Irregular”に分類し対比検討を行った（Fig. 1）．統計学的な有意差の検定は，統計ソフトはJMP version8.0.1（J, SAS Institute, Cary, NC, USA）を用いStudent's t-test，Wilcoxonの検定およびFisher's exact testで行った．

結果：42結節の組織学的分化度は高分化15結節（22.4±14.9 mm），中分化23結節（29.1±24.6 mm），低分化4結節（29.2±24.3 mm）であった．またMFIパターンでみるとFine 13結節（31%），Vascular 26結節（62%），Irregular 3結節（7%）であった．これらを対比検討すると，高分化15結節のうち9結節（60%）がFineであり，Irregularは認めなかった．中分化23結節ではFine4結節（17%），Vascular18結節（78%），Irregular1結節（4%）とVascularが多かった．低分化4例はVascularとIrregularが2結節（50%）ずつであった．また動脈優位相で，多血性の有無の検討をしたが，高分化であっても11結節（73%）がhyperで，組織型の推定には有効ではなかった．しかしKupffer相では低分化の全例がhypo，高分化では8結節53%がisoであり組織型を反映していた．そこでKupffer相とMFI所見と組み合わせた5段階のHCC造影US悪性度分類を考案し，組織所見と比較検討した．結果，組織学的に中低分化型HCCの占める割合はiso-Fine 0%（0/6），iso-Vascular 50%（2/4），hypo-Fine 57%（4/7），hypo-Vascular 82%（18/22），Irregular 100%（3/3）の順に増した（Table 1）．統計学的にもGrade IIではGrade

1）兵庫医科大学超音波センター
2）兵庫医科大学肝胆膵内科
3）兵庫医科大学病院病理部
4）兵庫医科大学病理学講座分子病理部門
5）兵庫医科大学肝胆膵外科
*Corresponding author: hiroko-i@hyo-med.ac.jp
＜受付日2009年1月9日＞＜採択日2009年4月28日＞

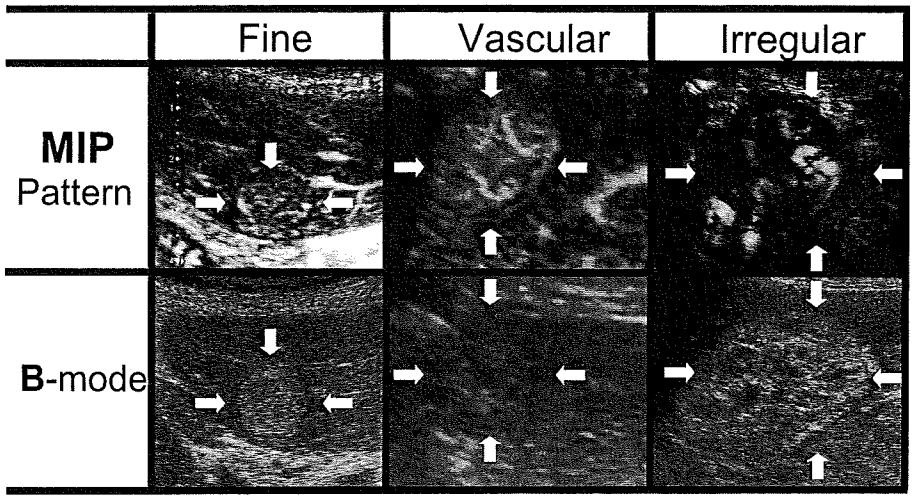

Fig. 1 Maximum intensity projection (MIP) pattern is classified as one of the following three patterns: fine, vascular, irregular patterns. In the fine pattern, so-called tumoral vessels were not clearly visualized and only fine vessels were visualized. When the vascular architecture in the tumoral region was similar to that in the adjacent non-tumoral region, it is also classified as fine pattern. In the vascular pattern, tumoral vessels were visualized clearly. In the irregular pattern, tumoral vessels were thick and irregular.

Table 1 Contrast enhanced ultrasonography classification of HCC

Grade	Kupffer phase	MIP	n	mean size (mm)	well	moderate	poor	moderate and poor
I	iso	Fine	6	21.7±7.7	6	0	0	0% (0/6)
II		Vascular	4	19.7±13.6	2	2	0	50% (2/4)*
III	Hypo	Fine	7	13.6±6.4	3	4	0	57% (4/7)
IV		Vascular	22	27.6±18.8	4	16	2	82% (18/22)
V		Irregular	3	67.0±44.6	0	1	2	100% (3/3)

MIP: Maximum Intensity Projection, well: well differentiated hepatocellular carcinoma, moderate: moderate differentiated hepatocellular carcinoma, poor: poor differentiated carcinoma *Significantly different from the result obtained in grade I (P = 0.049)

Iに比べ中低分化の割合が有意に増加しており（P＝0.049），またGrade VではGrade IVと比較し低分化が多い傾向を認め（P＝0.057），この分類は組織学的悪性度を反映していた．従来のBモード像やサイズでも同様に比較検討したところ，Grade VではGrade IVと比較して有意に腫瘍径が大きかったが（P<0.001），これらの因子による悪性度の層別化はできなかった．

考察：HCCのサーベイランスが発達し，2 cm未満のHCCが多く発見されRFAなどの局所治療が一般的に行われるようになった現在，組織学的悪性度のみならず生物学的な悪性度を評価することは，治療方針を決定する上で重要である．Sonazoid CEUSは簡便，低侵襲かつリアルタイムに血流を診断でき，更にMIPにより血管形態やKupffer相を評価することができる．昨年より利用可能となったEOB-MRIプリモビストも血管相と肝細胞相を評価でき，期待がもたれているが[5]，超音波と比較し，簡便性・分解能の点から詳細な腫瘍血管

の評価は困難である．

同じ第二世代の造影超音波剤である SonoVue を用いた MFI での肝癌の分化度を検討した報告はあるが[6][7]，わが国では SonoVue の保険適応がない．また MFI 所見のみの診断は読影者による不一致が見られやすい[6]．今回我々の提唱する診断法は，より簡素化した MIP 所見と Kupffer 相を相補的に用いることで客観性を高めた．またより明快な分類名称が望ましいと考え，判定しやすい名称を提案した．

今回の検討で，CEUS の動脈相が hyper にも関わらず，Kupffer 相で iso となっている結節を認めた．これは，症例のすべてが切除症例ではないため腫瘍全体の組織分化度を反映していない可能性は否めない．さらに慢性肝疾患や脂肪肝など背景肝の影響も一因である可能性がある．これらは今後の CEUS の課題と考えられた．

結論：今回我々の報告した Sonazoid による肝癌悪性度分類法は，非侵襲的に肝癌の悪性度評価を可能とし得る有用な方法と考え提唱する．

索引用語：造影超音波，悪性度分類，肝細胞癌

文献：1) Hayashi M, Matsui O, Kadoya M, et al. Radiology 2002; 225: 140—143　2) Ueda K, Terada T, Matsui O, et al. Hum Pathol 1992; 23: 619—626　3) Nakamura K, Zen Y, Nakamura Y, et al. Hum Pthol 2007; 38: 1532—1546　4) Tanaka M, Nakashima O, Kojiro M, et al. Hepatology 1999; 24: 807—812　5) Reimer P, Schnerder G, Schima W. Eur Radiol 2004; 14: 559—578　6) Sugimoto K, Moriyasu F, Iijima H, et al. Hepatol Res 2008; 38: 790—799　7) Yang H, Liu GJ, Lu MD, et al. J Ultrasound Med 2007; 26: 461—467

英文要旨

New malignancy grading system for hepatocellular carcinoma using Sonazoid contrast enhanced ultrasonography

Hironori Tanaka[1)2)], Hiroko Iijima[1)2)*], Masaki Saito[2)], Nobuhiro Aizawa[2)], Yoshiyuki Sakai[2)], Syohei Yoshikawa[2)], Teruhisa Yamamoto[2)], Hirayuki Enomoto[2)], Yoshinori Iwata[2)], Noritoshi Kou[2)], Hiroyasu Imanishi[2)], Soji Shimomura[2)], Hideji Nakamura[2)], Seiichi Hirota[3)], Toru Tujimura[4)], Jiro Fujimoto[5)], Shuhei Nishiguchi[2)]

We investigated the clinical utility of a new grading system for malignant hepatocellular carcinoma (HCC) using a combination of two different contrast-enhanced ultrasonographic (CEUS) images. 33 patients with histologically confirmed 42 HCC nodules (well-differentiated, n = 15; moderately-differentiated, n = 23; poorly-differentiated, n = 4) received CEUS. Kupffer phase and Maximum Intensity Projection (MIP) images were classified respectively by their patterns as follows: Kupffer images (i) hyper; (ii) iso; (iii) hypo; MIP findings (i) Fine; (ii) Vascular; (iii) Irregular. Based on the combination of these two images, they were classified into five grades. The correlation between this new and the histological grading showed that this new grading system could predict moderate- and poorly-differentiated HCC; iso-Fine 0%, iso-Vascular 50%, hypo-Fine 57%, hypo-Vascular 82%, Irregular 100%.

Key words: ultrasonography, malignancy grading system, hepatocellular carcinoma

Kanzo 2009; 50: 397—399

1) Ultrasonography Center, Hyogo College of Medicine
2) Division of Hepatobiliary and Pancreatic Disease, Department of Internal Medicine, Hyogo College of Medicine
3) Department of Radiology, Hyogo College of Medicine
4) Department of Surgical Pathology, Hyogo College of Medicine
5) Division of Hepatobiliary and Pancreatic Medicine, Department of external Medicine, Hyogo College of Medicine
*Corresponding author: hiroko-i@hyo-med.ac.jp

Ultrasound in Med. & Biol., Vol. 35, No. 11, pp. 1819–1827, 2009

0301-5629/09/$–see front matter

ELSEVIER

doi:10.1016/j.ultrasmedbio.2009.05.013

● *Original Contribution*

DEFINITION OF CONTRAST ENHANCEMENT PHASES OF THE LIVER USING A PERFLUORO-BASED MICROBUBBLE AGENT, PERFLUBUTANE MICROBUBBLES

SASAKI SHUNICHI,* IIJIMA HIROKO,† MORIYASU FUMINORI,* and HIDEHIKO WAKI‡

*Department of Gastroenterology and Hepatology, Tokyo Medical University, Tokyo; †Division of Hepatobiliary and Pancreatic Medicine, Department of Internal Medicine, Hyogo College of Medicine, Hyogo; and ‡Ultrasound Imaging Center, Hyogo College of Medicine, Hyogo, Japan

(*Received* 22 *May* 2008, *revised* 12 *May* 2009, *in final form* 18 *May* 2009)

Abstract—To define the contrast enhancement phases in the liver with perflubutane microbubbles, the liver enhancement time-intensity curves were investigated in 14 healthy volunteers. The agent was injected intravenously as a bolus and the liver was imaged with an ultrasound scanner as long as 4 h after the injection. Time-intensity curves from the hepatic artery, the intrahepatic portal vein, the hepatic vein and the parenchyma of the liver were obtained from the liver ultrasound images. The arrival of the agent in the hepatic artery, the portal vein and the hepatic vein were visually distinguishable and the mean arrival times were 19.2, 24.3 and 32.2 s after the injection, respectively. The signal intensity in these vessels increased rapidly after the arrival of the contrast and gradually reverted to baseline after the peak. In contrast, within 5 min after the injection, the intensity in the parenchyma increased and reached a plateau, which persisted for at least 2 h. The contrast enhancement phases in the liver with perflubutane microbubbles could be defined as two major phases—a vascular phase, in which the vessels are enhanced between 15 s and 10 min after injection, and a Kupffer phase, in which the parenchyma is enhanced 10 min after injection. The vascular phase is divided into three subphases: the arterial phase (15 to 45 s after injection); the portal phase (45 s to 1 min after injection); and the vasculo-Kupffer phase (1 to 10 min after injection). (E-mail: hiroko-i@hyo-med.ac.jp) © **2009 World Federation for Ultrasound in Medicine & Biology.**

Key Words: **Perflubutane microbubbles, Contrast ultrasound, Time-intensity curves, Vascular phase, Kupffer phase, Sonazoid.**

INTRODUCTION AND LITERATURE

In addition to contrast-enhanced X-ray/computed tomography (CT) and magnetic resonance imaging (MRI), contrast-enhanced ultrasonography has become the new standard method for the diagnosis of liver focal lesions (Lencioni 2006; Nicolau et al. 2006; Leen et al. 2006). Different from the iodinated agent used in X-ray/CT and the gadolinium chelating agent used in MRI, the ultrasound contrast agent, which consists of microbubbles (MB), cannot be distributed into the interstitium through the vascular endothelium; this means that the MB contrast agent used in ultrasonography is a true blood pool agent (Burns and Wilson, 2007). Therefore, the pharmacodynamics of ultrasound contrast agents may not be the same as the pharmacodynamics of agents for X-ray/CT and MRI. In contrast-enhanced X-ray/CT and MRI, the time-intensity curves (TIC) of the hepatic vessels and parenchyma have been well studied, and the contrast phases, such as the arterial, portal and equilibrium phases, have been well defined and introduced in routine clinical settings (Atasoy and Akyar 2004; Gandhi et al. 2006; Winterer et al. 2006).

In our previous study, we described and defined the contrast enhancement phases of the liver with an air-based MB agent (Levovist; Nihon Shering, Tokyo, Japan) in healthy volunteers by investigating TIC of the aorta, the portal vein and hepatic parenchyma (Iijima et al. 2007). Recently, perfluoro-based MB agents, which have better stability and resistance to pressure, were developed by changing the gas to a lower solubility substance (Schutt et al. 2003). The transit time of contrast ultrasonography with perfluoro-based MB agents in patients with liver disease has been studied (Albrecht et al. 1999;

Address correspondence to: Iijima Hiroko, 1-1 Mukogawa-cyo, Nishinomiya, Hyogo 663-8501, Japan. E-mail: hiroko-i@hyo-med.ac.jp

Lim et al. 2006; Blomley et al. 2003). Because of the high temporal and spatial resolution of ultrasonography, contrast-enhanced ultrasonography with perfluoro-based MB agents can visualize the vasculature and perfusion of the lesions continuously, which has resulted in high accuracy in characterizing lesions (Jang et al. 2007; Wilson et al. 2008). However, it is known that disposition of the MB agents, even among the perfluoro-based agents, differs with the composition of the gas and shell materials (Hutter et al. 1999; Toft et al. 2006). Therefore, investigating the dynamics of respective MB agents in the liver is of great significance for the standardization of liver contrast ultrasonography.

The perflubutane MBs (Sonazoid™; Daiichi Sankyo, Tokyo, Japan) used in this study are newly launched and commercially available in Japan (Moriyasu 2004; Matsumura and Sugihara 2007). This agent provides two different phases of contrast enhancement in the liver: vascular and Kupffer phase imaging (Moriyasu 2004; Watanabe et al. 2003). The former phase occurs shortly after intravenous injection of the agent, which allows depicting the vasculature of hepatic lesions based on the dynamics of the agent. The latter phase is a parenchyma-specific contrast in the liver, typically occurring 10 min after the injection. Because malignant hepatic tumors contain few or no Kupffer cells, the malignant lesions are depicted as a clear contrast defect, resulting in improved lesion detection (Moriyasu 2004; Forsberg et al. 2002).

To define its liver enhancement phases, we investigated the pharmacodynamics of the agent in the liver using healthy volunteers by creating TIC of the ultrasound contrast enhancement.

MATERIALS AND METHODS

Contrast agent

Perflubutane MBs are MBs of gaseous perflubutane (C_4F_{10}) stabilized with a monomolecular membrane of hydrogenated egg phosphatidyl serine (Sontum 2008). The lyophilized formulation is suspended with 2 mL of water, where each milliliter of the suspension contains 8 μL of perflubutane MBs.

Subjects

This study was approved by the institutional review board. All subjects gave informed consent. All subjects fasted for 6 h or more before the contrast ultrasonography. This study included healthy volunteers ≥20 years old. There were no special exclusion criteria. A total of 14 healthy volunteers were enrolled in this study. For the vascular phase evaluation, there were three males and three females. Their age, body weight and height ranged from 24–44 years old (mean 35.8), 46–82 kg (mean 61.8) and 150–186 cm (mean 164.3), respectively. For the Kupffer phase evaluation, there were five males and three females. Their age, body weight and height ranged from 30–44 years old (mean 37.1), 53–89 kg (mean 63.1) and 161–181 cm (mean 167.5), respectively.

Contrast ultrasonography

Perflubutane MBs were injected intravenously as a bolus through a 21-gauge needle placed in the medial vein of the left arm. We used an extension tube (1.0 mL) for the injection and, initially, the MBs were introduced into the extension tube to avoid premature injection into the vein. Then, the agent was injected at a rate of 1 mL/s, followed by a flush of 10 mL saline at the same injection rate. The time-clock was started at the same time as the saline flush.

The ultrasound equipment used was Aplio™ (Toshiba Medical Systems Corp., Ohtawara, Japan) equipped with a convex probe (PVT-375BT). The imaging mode used to assess the vascular phase was pulse subtraction harmonic imaging (PSHI), which used positive and inverted pulses to retrieve the nonlinear signals from the MBs. Low acoustic power with a mechanical index (MI) of 0.1–0.4 was used and the frame rate was 10–12 frames per second. For the Kupffer phase, the advanced dynamic flow (ADF) mode, which uses a wide-band Doppler technique, was used at a high acoustic power (MI 1.6) for loss of correlation imaging. Digital images both for the vascular and Kupffer phases were stored on the hard drive of the scanner for subsequent image analysis.

Vascular phase imaging and analysis

The image plane that simultaneously contained the hepatic artery, hepatic vein and portal vein was selected. Digital images were recorded on the hard disk of the ultrasound equipment for 30 min after an injection of 7.5×10^{-3} mL/kg of the agent in suspension, which contained 6.0×10^{-2} μL/kg perflubutane MBs. The subjects were asked to breathe gently throughout the scanning procedure. In the subsequent image analysis, we calculated TIC using ImageLab Avi (Toshiba Medical Systems Corp., Ohtawara, Japan) on the offline computer, which is PC-based software dedicated to analyzing ultrasound images.

The regions-of-interest (ROIs) were set on the vascular space of the hepatic artery, the portal vein and the hepatic vein for measuring their signal intensity (Fig. 1). ROIs were measured at time zero and every 1 s up to 1 min (1 to 60 s), then every 15 s up to 3 min (75, 90, 105, 120, 135, 150, 165 and 180 s), then every 1 min up to 30 min (4 to 30 min). Each ROI was adjusted manually for the vascular space, because the image plane shifts during breathing. A 10% rise in signal intensity was used for the arrival times, which started from the injection

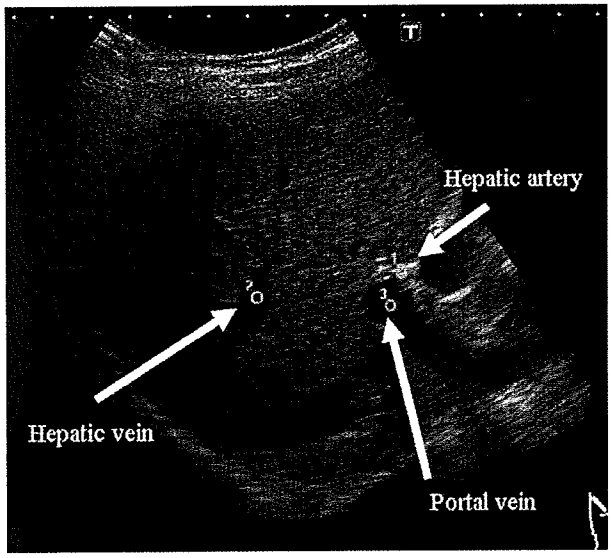

Fig. 1. Vascular phase. The ROIs are set in the hepatic artery, the portal vein and the hepatic vein to measure the signal intensity.

of the agent. The time-to-peak was defined as the time to reach the highest intensity from start of the injection. Differences in the arrival time among the hepatic artery, the portal vein and the hepatic vein were compared using a two-sample *t*-test approach at the 5% level of significance.

Kupffer phase imaging and analysis

The liver scanning was performed once at each of the nine time points (0, 5, 10, 20 and 40 min, and 1, 2, 3 and 4 h) after the injection of 1.5×10^{-5} mL/kg of the agent in suspension, which contained 1.2×10^{-4} μL/kg of perflubutane MBs. This dose was quite low, at one five-hundredth of that used for the vascular phase imaging, and the contrast signal was high in ADI mode because of destruction of the MBs with high MI, which meant that a lower dose was optimal for Kupffer phase imaging. Each scan was performed on different portions of the liver to avoid destructive effects on the MBs within the liver parenchyma. The left lobe was scanned in five different planes with a sagittal scan and a transverse scan, and the right lobe was scanned in five different planes including a subcostal scan and an intercostal scan. Each scan was designed to not overlap with any of the others. The subjects were asked to hold their breath during each scan. The still images of the parenchyma were recorded on the hard disk of the ultrasound equipment using a digital format. ImageLab (Toshiba Medical Systems Corp., Ohtawara, Japan) on the offline computer was used for subsequent analysis. Three different ROIs were set at the same focus points on the liver parenchyma to measure the signal intensity, and the mean values were used for the TICs (Fig. 2) to minimize the variations.

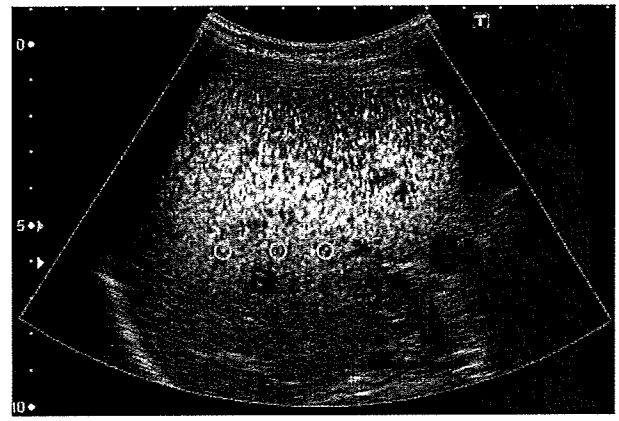

Fig. 2. Delayed parenchymal phase using ADF mode. ADF mode can depict the signals separately from the fundamental B-mode signals with this system. The ROIs are set in the liver parenchyma to measure the signal intensity.

RESULTS

Vascular phase

The arrival of the agent in the hepatic artery, the portal vein and the hepatic vein was visually distinguishable (Fig. 3). The arrival time and time-to-peak intensity in the hepatic artery varied from 14–25 s after injection (mean 19.2 ± 4.4 s SD) and from 23–42 s (mean 33.5 ± 8.1 s SD), respectively. The arrival time and time-to-peak intensity at the portal vein varied from 20–30 s after injection (mean 24.3 ± 4.2 s SD) and from 34–48 s (mean 41.5 ± 6.2 s SD), respectively. The arrival time and time-to-peak intensity at the hepatic vein varied from 23–43 s after injection (mean 32.2 ± 6.9 s SD) and from 50–69 s (mean 59.8 ± 6.1 s SD), respectively. The mean difference in the arrival time between the hepatic artery and the portal vein was 5.17 s ($p < 0.0001$); between the hepatic artery and the hepatic vein 13.0 s ($p < 0.0006$); and between the portal vein and the hepatic vein was 7.83 s ($p < 0.0067$). The point where the portal vein and the hepatic artery intersect in the TIC was 45 s (Fig 5).

Figure 4 shows the TICs of the hepatic arteries, the portal veins and hepatic veins from all the subjects, whereas Fig. 5 shows the curves with their mean values.

Kupffer phase

The intensity of parenchyma rapidly increased and reached a plateau at 5 min, which lasted for 2 h after injection of the agent (Fig. 6). The average time to maximum intensity of the parenchyma was about 40 min after injection. Typical images of the parenchyma enhancement at each time point are shown in Fig. 7. The parenchymal enhancement was well depicted and the signals separated from the background B mode.

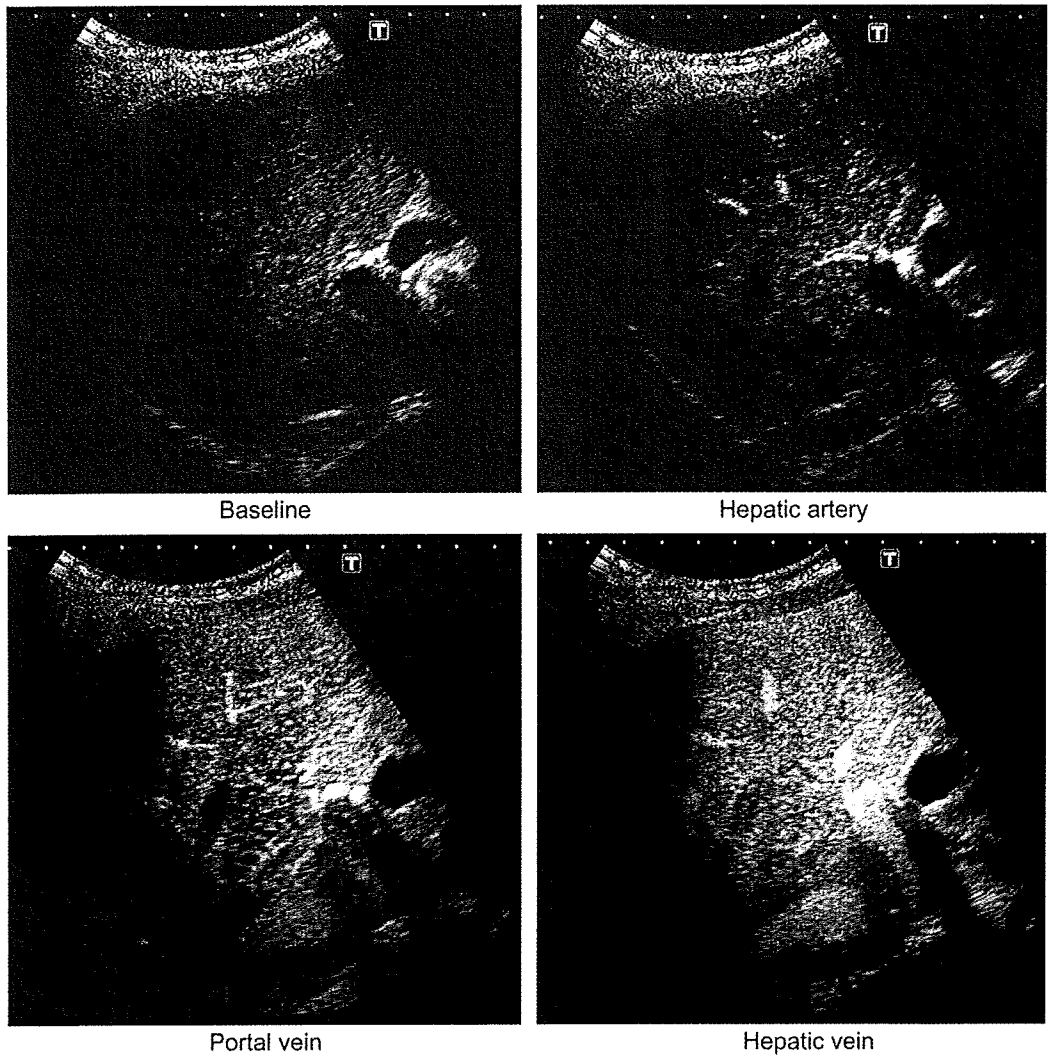

Fig. 3. Contrast enhancements of the hepatic vessels.

DISCUSSION AND SUMMARY

In this study, we investigated TICs of liver enhancement with perflubutane MBs and defined the liver enhancement phases.

Contrast ultrasonography and image analysis

Of 14 volunteers, six subjects were enrolled in the vascular phase evaluation, and eight were in the Kupffer phase. Because the endpoints between the vascular phase and the Kupffer phase were different, we conducted two separate examinations. In addition, some MBs are destroyed during the vascular phase because of the ultrasound transmission; thus, we conducted two separate examinations to measure the pure contrast phase. Therefore, the number of subjects was different for the two phases.

For the injection procedure, we used an extension tube so that, initially, the MBs did not enter the vein. The time of injection (time 0) was at the same time as the saline flush.

PSHI was used for the vascular phase and ADF was used for the delayed parenchymal phase. The reason for using different imaging techniques for the vascular and Kupffer phases was as follows. Vessels in the liver are acoustically translucent, so that the signal intensity of vessels at baseline is low enough to measure signals from the MBs quantitatively. Therefore, PSHI with low MI was suitable to obtain continuous images. On the other hand, tissue background signals of liver parenchyma at baseline were not suppressed enough with PSHI, so we used ADF instead of PSHI. A Doppler-like mode could have suppressed the tissue background; however, the image planes had to be changed at different time points because of the destruction of MBs with high MI of ADF.

Because the hepatic artery, the portal vein and the hepatic vein are quite small and large ROIs detect signals

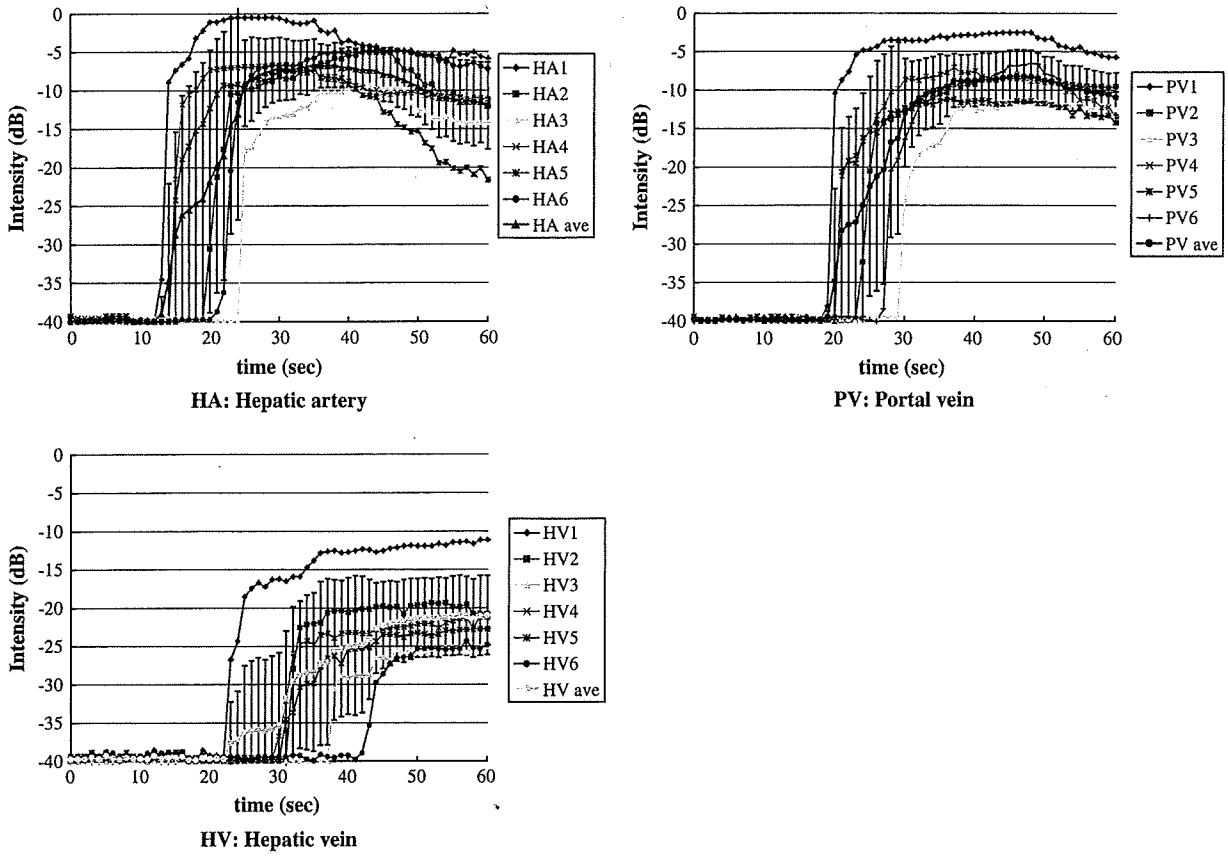

Fig. 4. Time-intensity curves of the hepatic artery, the portal vein and the hepatic vein from all subjects.

from the surrounding tissue, we used small ROIs to measure the intensity of the vessels. In addition, the hepatic artery is small compared with the other hepatic veins, such that the time-intensity of the hepatic artery is susceptible to respiration effects. This factor may cause substantial variance in the ascending part of the artery arrival curves. The time-to-peak was measured in addition to the arrival times of the hepatic veins. The time-to-peak shows a sharper curve than the arrival time and provides information for the understanding of the ultrasound contrast phases.

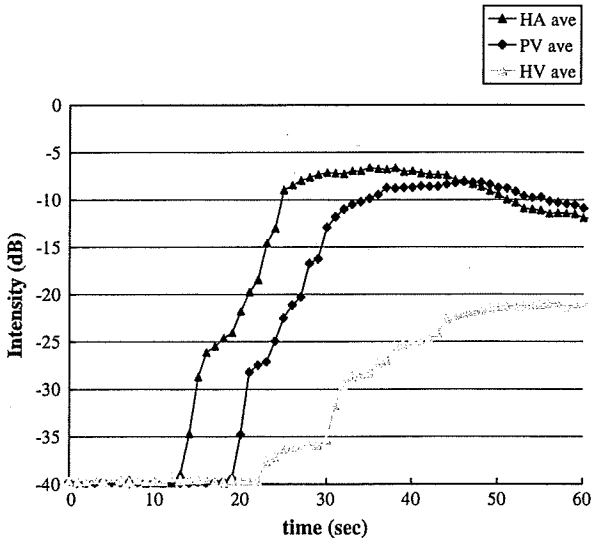

Fig. 5. Average time-intensity curves of the hepatic artery, the portal vein and the hepatic vein.

Vascular phase

The vascular phases of X-ray/CT and MRI in the liver have been categorized into three phases: early, late and delayed (equilibrium) phases (Heiken et al. 1993). Vascular phases with Sonazoid ultrasonography could be categorized into three subphases: arterial, portal and vasculo-Kupffer. This is similar to conventional contrast studies in digital subtraction angiography, X-ray/CT and MRI. The vascular phase of ultrasound contrast imaging is clinically useful in the diagnosis of tumor vascularity, thrombosis, tumor thrombus and portal venous abnormalities (Fan et al. 2006).

There were variations in the arrival time in this study, with some possible explanations being: (i) error in the injection procedure; (ii) interindividual variability (individual differences); or (iii) intraindividual variability

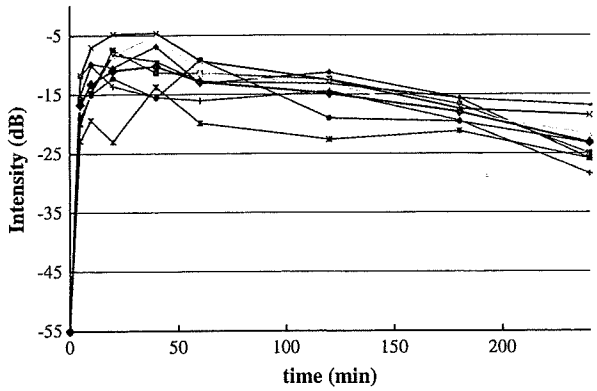

Fig. 6. Time-intensity curve of contrast enhancement of the liver parenchyma at each scanning point time (*red line* shows the average).

(subject conditions). In this study, the injection procedure was unified and carefully maintained and these factors were unlikely to affect the variation. Similar variations in the arrival times were reported for X-ray/CT studies. Kopka et al. (1996) reported that there was a variation of the aorta arrival time from 7–25 s in X-ray/CT and that the differences were not statistically dependent on gender, age, blood pressure, body weight or injection speed. Therefore, individual differences or patient conditions might be the cause of the arrival time variation; however, further reasons or parameters for this variation could not be specified.

Differences in perflubutane MBs from other agents

Contrast ultrasound examination with perflubutane MBs showed similar arrival times in the arterial and portal vein when compared with our previous study on air-based MBs. Concerning the Kupffer phase, perflubutane MBs showed a longer enhancement period than air-based MBs. Parenchyma-specific contrast enhancement lasted at least 2 h in the human subjects in this study, where this would be defined as the Kupffer phase. Although perflubutane MBs provide more than 2 h of useful contrast enhancement of the liver parenchyma, with air-based MBs less than 1 h enhancement was achieved (Iijima et al. 2007). This finding was quite reasonable because perflubutane MBs are more stable than air-based MBs, and perflubutane MBs have been demonstrated to exist as MBs without digestion by Kupffer cells for a longer time (Watanabe et al. 2007). In addition, shell composition plays a more important role in the protection of gas release from the inside of the MBs. Microbubbles stabilized with lipid, which is also used as a stabilizer for perflubutane MBs, are more stable in cells stabilized with albumin (Lindner et al. 2000).

The dynamics of blood circulation should correlate with the disposition of perflubutane MBs, so that the disposition of perflubutane can be investigated precisely in laboratory animals (Toft et al. 2006). When the agent was injected into rats, the half-life of perflubutane in the blood was less than 5 min. However, in the liver, it was about 3–4 h, with 30–40% of the injected dose remaining

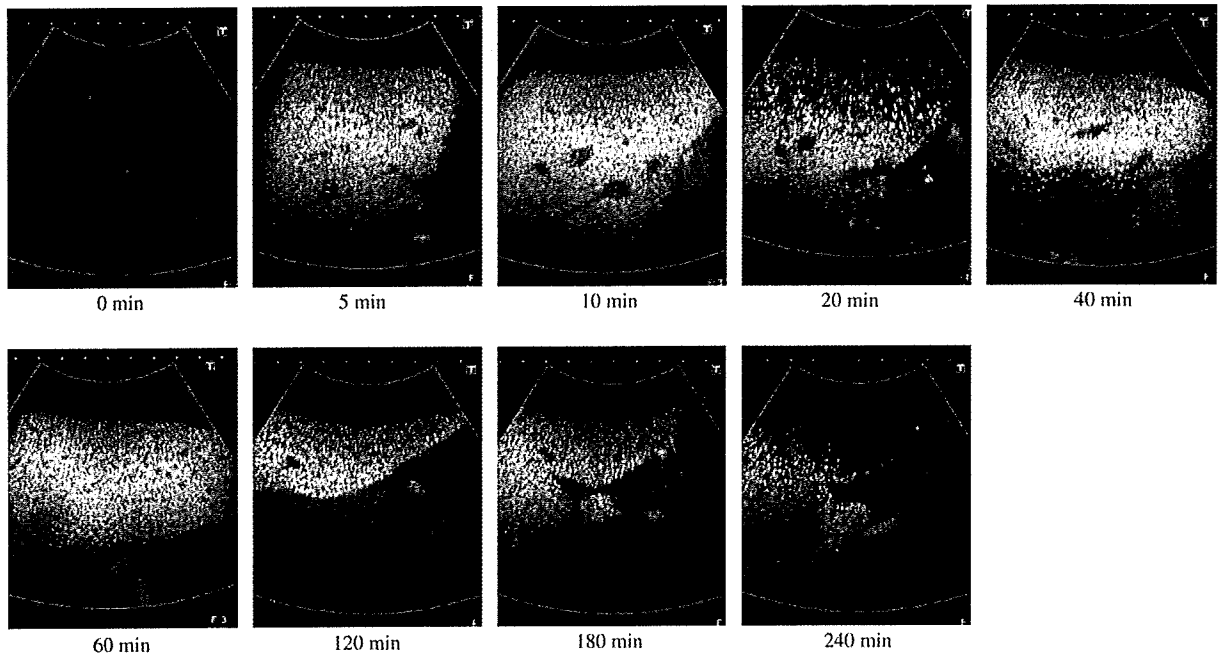

Fig. 7. Images of the Kupffer phase of the liver parenchyma at each scanning point time.

Table 1. Definition and the name of the perflubutane MB ultrasound contrast phases

Vascular phase
The vascular phase is divided into three phases • Arterial phase (15–45 s after injection) The time from the arrival of perflubutane microbubbles in the hepatic artery to the point where the portal vein and the hepatic artery intersect in the TIC • Portal phase (45 s – 1 min after injection) The time from the point when the hepatic arterial and the portal vein intersected in the TIC to the point where the portal vein and the parenchyma intersect in the TIC • Vasculo-Kupffer phase (1–10 min after injection) The time from the point when the portal vein and the parenchyma intersect in the TIC to the disappearance of the contrast effect from the vasculature Kupffer phase (from 10 min after injection) • The time when the parenchyma of the liver is enhanced after the disappearance of the contrast effect from the vasculature

The time is estimated based on the results.

in the liver at 20 min after injection. This retention in the liver was found to be a result of the uptake of the MBs by Kupffer cells in the sinusoidal space (Watanabe et al. 2007; Kindberg et al. 2003). The contrast enhancement phases of the liver seen in this study were in good agreement with the disposition of perflubutane in rats. Namely, the arterial and portal phase started shortly after the injection, then enhancement of parenchyma reached a plateau, whereas the enhancement in the vessels decreased.

Because X-ray/CT and MRI contrast agents are low-molecular-weight, water-soluble compounds and are extremely low in lipophilicity, these agents diffuse from the vascular space to the interstitium, but are not distributed into the cells (Heiken et al. 1993). In contrast, the mean sizes of the MB agents are similar to, or less than, red blood cells, but are not submicron in size. Therefore, the agents are retained in the vascular space. However,

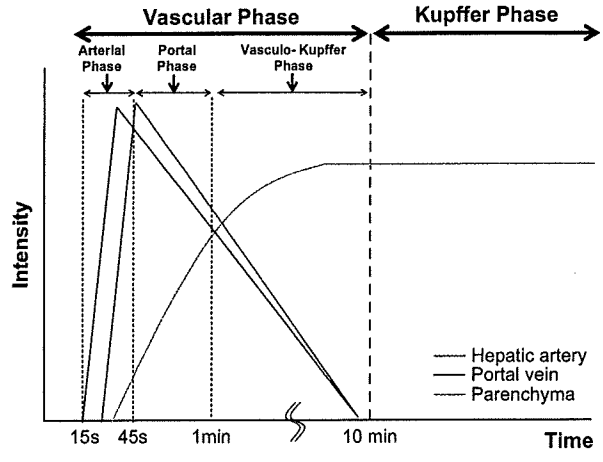

Fig. 8. Scheme for the perflubutane MB ultrasound contrast phases.

several MB agents are known to have liver parenchyma–specific contrast, in which parenchyma enhancement lasts after the wash-out of the agent from the bloodstream. The reason for the long-period enhancement with these MBs is believed to be phagocytosis of the MBs by Kupffer cells, which exist in the liver sinusoids (Yanagisawa et al. 2007). Therefore, the definition of the contrast-enhanced phase in X-ray/CT and MRI cannot simply be applied to contrast ultrasound of the liver.

Compared with air-based MBs, a continuous and longer imaging period is available with perflubutane MBs by using low acoustic power. In addition, the injection volume of perflubutane MBs is small; the injection volume of perflubutane MBs in clinical settings is 0.12 μL MB/kg (0.9 mL for patients with 60 kg body weight), whereas 5–7 mL would be injected for the air-based MBs. In addition, perflubutane MBs are stable for 2 h after being suspended in water, whereas the air MBs are less stable and are available for only 10 min after they have been suspended. Therefore, continuous and longer imaging windows and easy handling of perflubutane MBs would be meaningful improvements in the clinical settings.

The clearance of MB agents from the bloodstream is expected to be affected by their *in vivo* stability and phagocytosis of the agents by the reticuloendothelium system (RES), such as Kupffer cells. This means that phagocytosis by the RES is a key factor that primarily affects the disposition of MB agents resulting in the contrast patterns in the liver. In *in vitro* studies of perfluoro-based MB agents, perflubutane MBs and perflutren protein–type A microspheres (Optison; GE Healthcare, Princeton, NJ, USA) were phagocytosed, whereas perflutren lipid microspheres (Definity; Lantheus Medical Imaging, Inc., N. Billerica,

MA, USA), sulfur hexafluoride MBs (SonoVue; Bracco, Milan, Italy) and perflexane lipid microspheres (Imavist; Alliance Pharmaceutical Corp., San Diego, CA, USA) were not (Iijima et al. 2006; Yanagisawa et al. 2007). In the case of perflutren lipid microspheres and sulfur hexafluoride MBs, early washout of the contrast is often observed at the portal to the venous phase in malignant hepatocellular carcinoma (Jang et al. 2007). This is because the hepatic artery delivers 25% of the blood flow to the liver, and the portal vein delivers 75%. In contrast, malignant hepatic tumors have only a hepatic arterial blood supply and receive little or no flow from the portal vein. For those MBs not taken up by Kupffer cells, hepatic contrast enhancement mostly depends on the blood flow and concentration of the agent in the tumor and nontumorous liver tissue. However, in the case of perflubutane MBs, where phagocytosis of the MBs by Kupffer cells in the capillary beds of the liver sinusoid is believed to occur (Yanagisawa et al. 2007), parenchyma-specific contrast starts from arterial-portal phase, because the MBs flowing in the sinusoid are taken up by Kupffer cells without any delay. Therefore, elimination of the MBs from the bloodstream and accumulation in the liver parenchyma occur at the same time.

This vasculo-Kupffer phase should be a mixture of the vascular phase and the Kupffer phase; therefore, a pure Kupffer phase can be seen after the vascular contrast has been eliminated.

It is well known that the ability of Kupffer cells to phagocytose is depressed with severe cirrhosis or nonalcoholic steato-hepatitis (Tanimoto et al. 2002; Diehl. 2002). If a quantitative measurement of liver function using the contrast enhancement phases of perflubutane MBs could be established, this method could be meaningful in the evaluation of Kupffer function in patients with diffuse liver diseases (Moriyasu et al. 2005).

Limitations of this study

One of the limitations of this study was the subject population: we only used healthy volunteers and the number of subjects and their age ranges were small. Further study with a wide variation of healthy subjects will provide a more accurate baseline variation of the timings (arrival, peak, differences between phases). Therefore, in the future such reference timing would help to investigate the differences between normal subjects and the wide variations in patients with liver diseases.

Definition of contrast enhancement phases

The contrast enhancement phases of perflubutane MBs in the liver can be defined as follows (Table 1, Fig. 8.: The intensity levels for the vascular and Kupffer phases are derived from different types of measurements and so the levels are not directly comparable). There are two major phases: the vascular phase, in which the vessels are enhanced, is between 15 s and 10 min; the Kupffer phase, in which parenchyma is enhanced, which starts from 10 min after injection. The vascular phase is divided into three phases: the arterial phase (15 to 45 s after the injection), the portal phase (45 s to 1 min after the injection) and the vasculo-Kupffer phase (1 to 10 min after the injection).

Definition of the contrast enhancement phase for perflubutane MBs is important for the standardization of diagnosis using contrast enhancement ultrasound. Characterization of tumor lesions is performed by vascular phase imaging, and detection of the space occupying lesions is performed by Kupffer phase imaging.

REFERENCES

Albrecht T, Blomley MJ, Cosgrove DO, Taylor-Robinson SD, Jayaram V, Eckersley R, Urbank A, Butler-Barnes J, Patel N. Non-invasive diagnosis of hepatic cirrhosis by transit-time analysis of an ultrasound contrast agent. Lancet 1999;353:1579–1583.

Atasoy C, Akyar S. Multidetector CT: Contributions in liver imaging. Eur J Radiol 2004;52:2–17.

Blomley MJ, Lim AK, Harvey CJ, Patel N, Eckersley RJ, Basilico R, Heckemann R, Urbank A, Cosgrove DO, Taylor-Robinson SD. Liver microbubble transit time compared with histology and Child-Pugh score in diffuse liver disease: A cross sectional study. Gut 2003;52: 1188–1193.

Burns PN, Wilson SR. Focal liver masses: Enhancement patterns on contrast-enhanced images: Concordance of US scans with CT scans and MR images. Radiology 2007;242:162–174.

Diehl AM. Nonalcoholic steatosis and steatohepatitis IV. Nonalcoholic fatty liver disease abnormalities in macrophage function and cytokines. Am J Physiol Gastro Liver Physiol 2002;282:G1–G5.

Fan ZH, Chen MH, Dai Y, Wang YB, Yan K, Wu W, Yang W, Yin SS. Evaluation of primary malignancies of the liver using contrast-enhanced sonography: correlation with pathology. AM J Roentgenol 2006;186:1512–1519.

Forsberg F, Piccoli CW, Liu JB, Rawool NM, Merton DA, Mitchell DG, Goldberg BB. Hepatic tumor detection: MR imaging and conventional US versus pulse-inversion harmonic US of NC100100 during its reticuloendothelial system-specific phase. Radiology 2002;222: 824–829.

Gandhi SN, Brown MA, Wong JG, Aguirre DA, Sirlin CB. MR contrast agents for liver imaging: What, when, how. Radiographics 2006;26: 1621–1636.

Heiken JP, Brink JA, McClennan BL, Sagel SS, Forman HP, DiCroce J. Dynamic contrast-enhanced CT of the liver: Comparison of contrast medium injection rates and uniphasic injection protocols. Radiology 1993;187:327–331.

Hutter JC, Luu HM, Mehlhaff PM, Killam AL, Dittrich HC. Physiologically based pharmacokinetic model for fluorocarbon elimination after the administration of an octafluoropropane-albumin microsphere sonographic contrast agent. J Ultrasound Med 1999;18:1–11.

Iijima H, Moriyasu F, Miyahara T, Yanagisawa K. Ultrasound contrast agent, Levovist microbubbles are phagocytosed by Kupffer cells—In vitro and in vivo studies. Hepatol Res 2006;35:235–237.

Iijima H, Sasaki S, Moriyasu F, Suzuki S, Yoshida M, Horibe T, Tsuchiya K. Dynamic US contrast study of the liver: Vascular and delayed parenchymal phase. Hepatol Res 2007;37:27–34.

Jang HJ, Kim TK, Burns PN, Wilson SR. Enhancement patterns of hepatocellular carcinoma at contrast-enhanced US: Comparison with histologic differentiation. Radiology 2007;244:898–906.

Kindberg GM, Tolleshaug H, Roos N, Skotland T. Hepatic clearance of Sonazoid perfluorobutane microbubbles by Kupffer cells does not reduce the ability of liver to phagocytose or degrade albumin microspheres. Cell Tissue Res 2003;312:49–54.

Kopka L, Rodenwaldt J, Fischer U, Mueller DW, Oestmann JW, Grabbe E. Dual-phase helical CT of the liver: Effects of bolus tracking and different volumes of contrast material. Radiology 1996;201:321–326.

Lim AK, Patel N, Eckersley RJ, Goldin RD, Thomas HC, Cosgrove DO, Taylor-Robinson SD, Blomley MJ. Hepatic vein transit time of SonoVue: A comparative study with Levovist. Radiology 2006;240: 130–135.

Leen E, Ceccotti P, Kalogeropoulou C, Angerson WJ, Moug SJ, Horgan PG. Prospective multicenter trial evaluating a novel method of characterizing focal liver lesions using contrast-enhanced sonography. Am J Roentgenol 2006;186:1551–1559.

Lencioni R. European Federation of Societies for Ultrasound in Medicine and Biology (EFSUMB). Impact of European Federation of Societies for Ultrasound in Medicine and Biology (EFSUMB) guidelines on the use of contrast agents in liver ultrasound. Eur Radiol 2006;16: 1610–1613.

Lindner JR, Dayton PA, Coggins MP, Ley K, Song J, Ferrara K, Kaul S. Noninvasive imaging of inflammation by ultrasound detection of phagocytosed microbubbles. Circulation 2000;102:531–538.

Matsumura M, Sugihara H. Basic and clinical profile of perflubutane (Sonazoid powder for injection). Folia Pharmacol Jpn 2007;130: 393–420.

Moriyasu F. Phase III multicenter clinical trial of Sonazoid in Japan for the characterization and detection of focal liver lesions. Hepatology 2004;40(Suppl 1):707A.

Moriyasu F, Iijima H, Tsuchiya K, Miyata Y, Furusaka A, Miyahara T. Diagnosis of NASH using delayed parenchymal imaging of contrast ultrasound. Hepatol Res. 2005;33:97–99.

Nicolau C, Vilana R, Catala V, Bianchi L, Gilabert R, Garcia A, Bru C. Importance of evaluating all vascular phases on contrast-enhanced sonography in the differentiation of benign from malignant focal liver lesions. Am J Roentgenol 2006;18:158–167.

Schutt EG, Klein DH, Mattrey RM, Riess JG. Injectable microbubbles as contrast agents for diagnostic ultrasound imaging: the key role of perfluorochemicals. Angew Chem Int Ed Engl 2003;42:3218–3235.

Sontum PC. Physicochemical characteristics of Sonazoid™, a new contrast agent for ultrasound imaging. Ultrasound Med Biol 2008; 34:824–833.

Tanimoto A, Yuasa Y, Shinmoto H, Jinzaki M, Imai Y, Okuda S, Kuribayashi S. Superparamagnetic iron oxide-mediated hepatic signal intensity change in patients with and without cirrhosis: Pulse sequence effects and Kupffer cell function. Radiology 2002;222: 661–666.

Toft KG, Hustvedt SO, Hals PA, Oulie I, Uran S, Landmark K, Normann PT, Skotland T. Disposition of perfluorobutane in rats after intravenous injection of Sonazoid. Ultrasound Med Biol 2006;32: 107–114.

Watanabe R, Matsumura M, Chen CJ, Kaneda Y, Ishihara M, Fujimaki M. Gray-scale liver enhancement with Sonazoid (NC100100), a novel ultrasound contrast agent; detection of hepatic tumors in a rabbit model. Biol Pharm Bull 2003;26:1272–1277.

Watanabe R, Matsumura M, Munemasa T, Fujimaki M, Suematsu M. Mechanism of hepatic parenchyma-specific contrast of microbubble-based contrast agent for ultrasonography: Microscopic studies in rat liver. Invest Radiol 2007;42:643–651.

Wilson SR, Jang HJ, Kim TK, Iijima H, Kamiyama N, Burns PN. Real-time temporal maximum-intensity-projection imaging of hepatic lesions with contrast-enhanced sonography. AJR Am J Roentgenol 2008;190:691–695.

Winterer JT, Kotter E, Ghanem N, Langer M. Detection and characterization of benign focal liver lesions with multislice CT. Eur Radiol 2006;16:2427–2443.

Yanagisawa K, Moriyasu F, Miyahara T, Yuki M, Iijima H. Phagocytosis of ultrasound contrast agent microbubbles by Kupffer cells. Ultrasound Med Biol 2007;33:318–325.

Cancer Science
The official journal of the Japanese Cancer Association JCA

Bmi-1 gene is upregulated in early-stage hepatocellular carcinoma and correlates with ATP-binding cassette transporter B1 expression

Kathryn Effendi,[1,3] Taisuke Mori,[1,3] Mina Komuta,[1] Yohei Masugi,[1] Wenlin Du[1] and Michiie Sakamoto[1,2]

[1]Department of Pathology, School of Medicine, Keio University, Tokyo, Japan

(Received September 29, 2009/Revised October 24, 2009/Accepted November 1, 2009)

Overexpression of "stemness gene" *Bmi-1* has been identified in some solid tumors. We investigated *Bmi-1* expression in hepatocellular carcinoma (HCC) and ATP-binding cassette transporter B1 (*ABCB1*) as a new potential target for *Bmi-1*. *Bmi-1* was highly expressed in HCC cell lines and the most well differentiated cell line, KIM-1, showed the highest expression. Immunohistochemical, immunocytochemical, and immunoelectron microscopic analysis showed the Bmi-1 protein as having a high intensity of small dots within the nucleus which reflected concentrated sites of Bmi-1 repressive activity. Clear "dot-pattern" staining was observed in 24 of 37 (65%) well differentiated HCC (including 13 of 21 early nodules [62%]), in 32 of 71 (45%) moderately differentiated HCC, and 7 of 14 (50%) poorly differentiated HCC. A similar expression was not observed in non-cancerous background regions. High Bmi-1 expression was observed in the early and well differentiated HCC. Furthermore, overexpression and suppression of *Bmi-1* was followed by a respective increase and decrease in *ABCB1* expression. As with *Bmi-1*, high *ABCB1* expression was also observed in the early and well differentiated HCC. A strong correlation between *ABCB1* and *Bmi-1* mRNA expression was seen in HCC cell lines and clinical samples (Pearson's correlation coefficient 0.95 and 0.90, respectively). The *Bmi-1* gene is upregulated in HCC, and in particular is highly expressed in early and well differentiated HCC. The fact that this expression correlated with that of *ABCB1* suggests a new regulation target for *Bmi-1*, and gives new insight into early hepatocarcinogenesis mechanisms and potential targets for future HCC treatment. (*Cancer Sci* 2010)

Hepatocellular carcinoma (HCC) is the sixth most common malignancy in the world and still ranks as the third highest cause of cancer-related death globally.[1] Although individual risks for hepatocarcinogenesis, such as hepatitis viral infection, excessive alcohol intake, and non-alcoholic steatohepatitis are well established, a poor prognosis of HCC is still unavoidable due to the unclear mechanism of hepatocarcinogenesis. HCC is characterized by a multistage process of tumor progression,[2] and molecular changes, particularly in the early stage of HCC, have rarely been shown. The idea of using stem cell principles to understand tumor development and progression has emerged because they share similar characteristics. Recent reports on cancer stem cells or acquirement of stem cell-like properties in various tumors have greatly increased the possible connection of these cells in tumorigenesis.[3,4] *Bmi-1* was first identified as a proto-oncogene that cooperates with c-*myc* to generate mouse pre-B cell lymphomas.[5] Some reports show that *Bmi-1* might induce immortalization by regulating human telomerase reverse transcriptase (hTERT) expression,[6–9] and might play a role in tumorigenesis by acting as a negative regulator of the INK4a/ARF locus that encodes two important tumor suppressors in human cancer, *p16* and *p19*.[10,11] The overexpression of *Bmi-1* has been identified in lymphoma[12,13] and in a few solid tumors such as lung, colorectal, nasopharyngeal, bladder, and HCC.[9,14–18] Many reports mainly focus on *Bmi-1* expression in the advanced stages of cancer and its role in a poor prognosis. However, the exact mechanistic role of *Bmi-1* in tumorigenesis is not clear. In HCC, inactivation of *p16* expression, a well-known target of *Bmi-1*, is already observed in the early stages of hepatocarcinogenesis, due to methylation or an epigenetic mechanism.[19,20] This suggests that another target in the *Bmi-1* signaling pathway should exist. Therefore, we examined the involvement of the "stemness gene" *Bmi-1* and its new potential downstream target in hepatocarcinogenesis.

To our knowledge, there are no studies clearly showing a subcellular expression pattern of *Bmi-1* as a high intensity of small dots within the nucleus in cancer cells. Herein, we examined the expression patterns of *Bmi-1* in HCC cell lines and clinical specimens by immunohistochemistry, and these were confirmed with immunocytochemistry and immunoelectron microscopy. We also examined the expression levels of the ATP-binding cassette transporter B1 (*ABCB1*), listed as one of the genes upregulated after *Bmi-1* induction in bone marrow stromal cells.[6] We hypothesize the potential for *ABCB1* to be a new target for *Bmi-1*. Immunohistochemical staining and mRNA expression level of *ABCB1* were analyzed to investigate the correlation between *Bmi-1* and *ABCB1*.

Materials and Methods

Cell culture. The human HCC cell lines, PLC/PRF/5 and HepG2, were obtained from the American Type Culture Collection (Manassas, VA, USA). KIM-1, KYN-2, and Li7 were established as reported previously.[21] All the cells were grown in RPMI-1640 medium supplemented with 10% FBS, 100 U/mL penicillin, and 100 μg/mL streptomycin.

Tissue specimens of HCC. HCCs and corresponding non-cancerous liver tissue were obtained from 100 patients with 122 nodules (37 well differentiated [including 21 early], 71 moderately differentiated, and 14 poorly differentiated HCCs) who underwent surgical resection at Keio University Hospital (Tokyo, Japan) between 2003 and 2006. The specimens were fixed in 10% formalin and embedded in paraffin. Three pathologists evaluated the histological diagnosis according to the criteria set by the World Health Organization.[22] The histological grade for HCC where different types were found within the same nodule was determined by the predominant histological grade. Primary hepatocytes were harvested from the autopsy of a human fetal liver donor with signed, informed consent. The cells were resuspended in growth medium (10% FBS in DMEM, containing 0.1 mM non-essential amino acid and 0.1 mM sodium pyruvate solution; Gibco BRL, Grand Island, NY,

[2]To whom correspondence should be addressed.
E-mail: msakamot@sc.itc.keio.ac.jp
[3]These authors contributed equally to this work.

doi: 10.1111/j.1349-7006.2009.01431.x

USA), and were maintained at 37°C in a humidified atmosphere containing 95% air and 5% CO_2. This study was carried out with the approval of the Ethics Committee of Keio University School of Medicine.

Real-time quantitative RT-PCR. Real-time quantitative RT-PCR (qRT-PCR) analysis was carried out as previously reported,[6] at least three times, including a no-template negative control. A total of 15 (five well differentiated, seven moderately differentiated, and three poorly differentiated) HCC clinical samples were used. The primer sets were: *Bmi-1* forward, 5′-GAGGGTACTTCATTGATGCCACAAC-3′ and reverse, 5′-GCTGGTCTCCAGGTAACGAACAATA-3′; *ABCB1* forward, 5′-GAGGCCAACATACATGCCTTCA-3′ and reverse, 5′-GGC TGTCTAACAAGGGCACGA-3′.

Immunohistochemical and immunocytochemical analysis. Immunohistochemical staining was done on formalin-fixed, paraffin-embedded tissue sections. These were heated at 120°C in 0.01 mol/L sodium citrate buffer, pH 7.0, for 10 min before incubation with a mouse Bmi-1 antibody (1/200; Upstate Biotechnology, Lake Placid, NY, USA) and a multidrug resistance protein 1 (MDR1) antibody (1/200; Santa Cruz Biotechnology, Santa Cruz, CA, USA). Sections were then incubated with ImmPRESS antimouse Ig kit secondary antibody (Vector Laboratories, Burlingame, CA, USA), and stained with diaminobenzidine. For immunocytochemical analysis, KIM-1 cells were grown to confluence on glass slides, fixed, and washed. The slides were incubated with the Bmi-1 antibody (1/200) in PBS containing 1% BSA, followed by FITC-conjugated, antimouse Ig (1/400; Dako, Glostrup, Denmark). Staining was evaluated using the LSM 510 Meta confocal microscope (Carl Zeiss, Oberkochen, Germany). All staining analysis was done at least twice. We defined Bmi-1 staining criteria as follows: distributed diffusely with clear staining of the "dot-pattern" was scored 2+; distributed focally with weak staining of the dot-pattern was scored 1+; and an absence of the dot-pattern was considered negative. Evaluation criteria for ABCB1 were defined as follows: clear staining of irregular canalicular with cytoplasmic staining scored 2+; an irregular canalicular staining pattern scored 1+; and no staining was considered negative.

Immunoelectron microscopy. KIM-1 cells grown to confluence on glass slides were fixed in 4% formaldehyde and incubated overnight at 4°C with the Bmi-1 antibody (1/200). After rinsing they were treated with a mouse secondary antibody (1/100; Dako) for 3 h at room temperature, then re-fixed in 1% glutaraldehyde for 10 min. After further rinsing, the sections were stained with diaminobenzidine and post-fixed in 2% osmium tetroxide. The slides were dehydrated in graded alcohol, embedded in epoxy resin, and hardened at 60°C for 72 h. Ultrathin sections were cut with an ultramicrotome, stained with uranyl acetate and viewed under a JEOL 1200 EXII transmission electron microscope (Nihon Denshi, Tokyo, Japan).

Immunoblotting. PLC/PRF/5, HepG2, KIM-1, KYN-2, and Li7 cells were lysed in lysis buffer (50 mM Tris-HCL [pH 7.5], 150 mM NaCl, 5 mM EDTA, 1% NP-40, and complete protease inhibitors). Supernatants of the homogenates were subjected to NuPAGE (4–12% Bis-Tris gel; Invitrogen, Carlsbad, CA, USA) by electrophoresis, and transferred to PVDF membranes. Anti-Bmi-1 (1/500), anti-MDR1 (1/200), and anti-actin (1/1000; Sigma, St Louis, MO, USA) were hybridized to the membranes and detected with ECL Western blotting detection reagents (GE Healthcare, Amersham, UK).

Transfection-induced overexpression and RNA interference. Human Bmi-1 full coding cDNA was cloned from the KIM-1 cell line with RT-PCR and inserted into pcDNA53 (Invitrogen). This vector was transfected into the primary fetal hepatocytes using Lipofectamine LTX and positive expression vector-transfected cells were selected with G418 (Invitrogen), according to the manufacturer's instructions. For RNA interference, all purified and pre-annealed siRNA molecules were obtained from Takara Bio (Shiga, Japan). Two siRNA molecules were used, siBmi-1#1 and siBmi-1#2, with the targeted sequences 5′-AACAAUAACGAAUAGAAUUGA-3′ and 5′-AA GAAUUAUAACUGAUGAUGA-3′, respectively. Control (non-targeting sequence), unmodified siRNA duplex was also purchased from Takara Bio.

Statistical analysis. Data are expressed as mean ± SEM. The χ^2-test was used when appropriate to determine the correlations between clinicopathological variables and *Bmi-1* expression. The relative mRNA expression levels were compared using the unpaired *t*-test, and the Pearson's correlation coefficient test was also used. Statistical significance was defined as $P < 0.05$. All statistical analyses were carried out using Statcel software version 2.0 (OSM, Tokyo, Japan).

Results

***Bmi-1* expressed in HCC cell lines and distributed in high intensity, dot-pattern expression in nucleus.** To assess the potential role of *Bmi-1* in hepatocarcinogenesis, we examined *Bmi-1* expression in five human HCC cell lines using qRT-PCR and Western blot analysis. *Bmi-1* was highly expressed at both the mRNA and protein level. The most well differentiated HCC cell line, KIM-1, showed at least a three-fold higher level of expression of *Bmi-1*, compared with the other cell lines

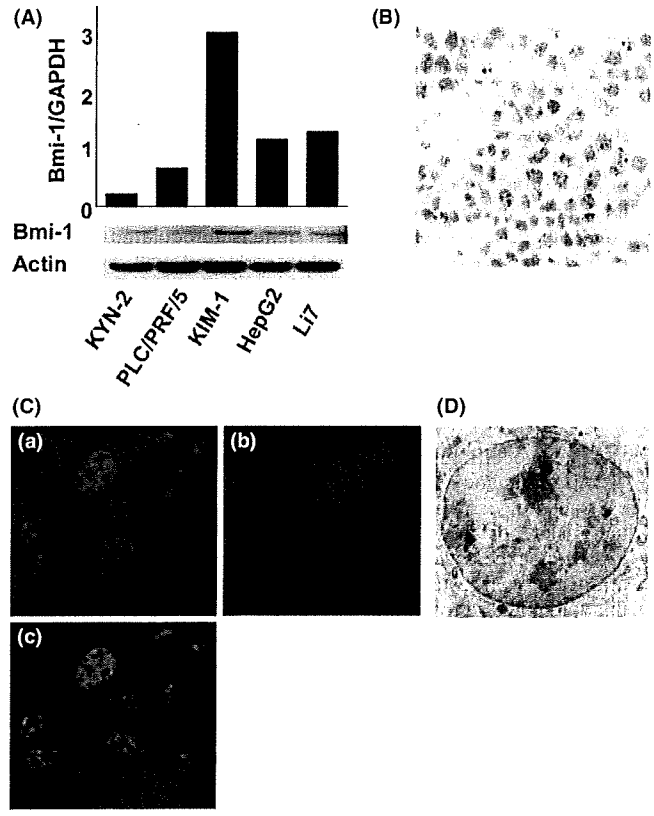

Fig. 1. *Bmi-1* expression in hepatocellular carcinoma (HCC) cell lines. (A) Quantitative real-time- PCR and Western blot of *Bmi-1* in HCC cell lines. *Bmi-1* is significantly expressed in the KIM-1 cell line compared with other cell lines. Nuclear fraction proteins were used in the Western blot analysis. Immunohistochemistry (B) and immuno cytochemistry (C) of KIM-1 cells. Bmi-1 was diffusely distributed intranuclearly (a, DAPI: blue; b, anti-Bmi-1: red; c, merged). (D) Immunoelectron micrograph of KIM-1. Bmi-1 particles are shown as small black dots inside the nucleus.

doi: 10.1111/j.1349-7006.2009.01431.x

(Fig. 1A). As a transcriptional repressor, Bmi-1 activity is expected in the nucleus, and we found Bmi-1 protein enrichment in the nuclear fraction compared with the whole lysates (data not shown). Immunohistochemistry, immunocytochemistry, and immunoelectron microscopic of the KIM-1 cells showed that the Bmi-1 protein was distributed in high-intensity aggregates within the nucleus (Fig. 1B–D). These results confirmed localization of the Bmi-1 protein in the nucleus, with a dot-pattern appearance.

***Bmi-1* expressed in HCC clinical samples, particularly in early stage hepatocarcinogenesis.** We evaluated Bmi-1 protein expression in 122 HCC nodules (37 well differentiated [including 21 early nodules], 71 moderately, and 14 poorly differentiated HCCs). As with Bmi-1 expression in the HCC cell lines, Bmi-1 expression in clinical samples was observed as small dots distributed inside the nucleus (Fig. 2A), but the Bmi-1 dot-pattern expression was not observed in the surrounding liver tissue (Fig. 2B). There was no correlation between expression of Bmi-1 and clinicopathological parameters, such as age, gender, portal involvement, intrahepatic metastasis, etiology, or non-cancerous background liver tissue. However, Bmi-1 positive expression was significantly associated with well (including early) differentiated HCC ($P = 0.023$) (Table 1). A 2+ score was observed in 24 of the 37 (65%) well differentiated HCCs (including 13 of the 21 early nodules [62%]), 32 of the 71 (45%) moderately differentiated HCCs, and 7 of the 14 (50%) poorly differentiated HCCs. In contrast, negative expression was observed in only 2 of the 37 (5%) well differentiated HCCs (including 2 of the 21 early nodules [10%]), 15 of the 71 (21%) moderately differentiated HCCs, and 4 of the 14 (29%) poorly differentiated HCCs (Table 2). Interestingly, a higher level of Bmi-1 expression was observed in the early and well differentiated HCCs, and this declined with the progression of HCC. Similar findings were found using qRT-PCR from clinical tissue samples. Strongly positive *Bmi-1* expression was observed in the five well differentiated HCC cases, compared with the seven moderately differentiated cases and the three poorly differentiated HCC cases (Fig. 2C). The average level of *Bmi-1* expression was significantly higher in tumor tissue compared with the non-cancerous background liver tissue (2.23 *vs* 0.86; $P = 0.002$).

***Bmi-1* expression linked to *ABCB1* expression.** We have previously analyzed gene expression profiles after *Bmi-1* induction in bone marrow stromal cells.[6] Among the genes upregulated we found that the *ABCB1* gene was upregulated together with the overexpression of *Bmi-1*, compared with the control parental cells (T. Mori *et al.*, unpublished observation, 2004). To further verify the regulation of *ABCB1* we looked at changes in *ABCB1* expression during transient overexpression of *Bmi-1* using primary fetal hepatocytes. Following *Bmi-1* overexpression, relative mRNA levels of *ABCB1* in primary fetal hepatocytes were increased threefold (Fig. 3A). *Bmi-1* knockdown also led to a downregulation of *ABCB1* expression in the KIM-1 HCC cell line (Fig. 3B), however, decreased *ABCB1* expression was not very significant, which might be due to the presence of *Bmi-1*-independent *ABCB1* expression. These results suggest a parallel association between *Bmi-1* and *ABCB1* expression in HCC cell lines and hepatocytes.

***ABCB1* expression in HCC cell lines and HCC clinical samples correlated with *Bmi-1* expression.** We further evaluated *ABCB1* expression in HCC cell lines and clinical samples. As with *Bmi-1*, the highest levels of ABCB1 mRNA and protein expression were observed in KIM-1 cells, relative to the other cell lines. *ABCB1* mRNA expression level in tumor tissue is not significantly higher compared with non-cancerous background liver tissue due to its normal expression in non-cancerous background liver tissue, however, there is a tendency for higher expression level of *ABCB1* in well differentiated cases (2.30 *vs* 1.53; $P = 0.21$) (Fig. S1a,b). We found a strong statistical correlation between *ABCB1* and *Bmi-1* mRNA expression with the Pearson's correlation coefficient being 0.95 and 0.90 for HCC cell lines and HCC clinical samples, respectively (Fig. 4A,B). Immunohistochemical staining of ABCB1 showed both cytoplasmic and a canalicular staining pattern in the tumor region. Although the canalicular staining pattern was also seen in the surrounding non-cancerous region, the pattern was more irregular and thicker (Fig. S1c,d). A 2+ score was observed in 29 of 37 (78%) well differentiated HCCs (including 18 of 21 early differentiated nodules [86%]), in 50 of 71 (70%) moderately differentiated HCCs, and in 10 of 14 (71%) poorly differentiated HCCs. Negative expression was observed in 1 of 37 (3%) well differentiated HCCs (no early nodules had negative expression),

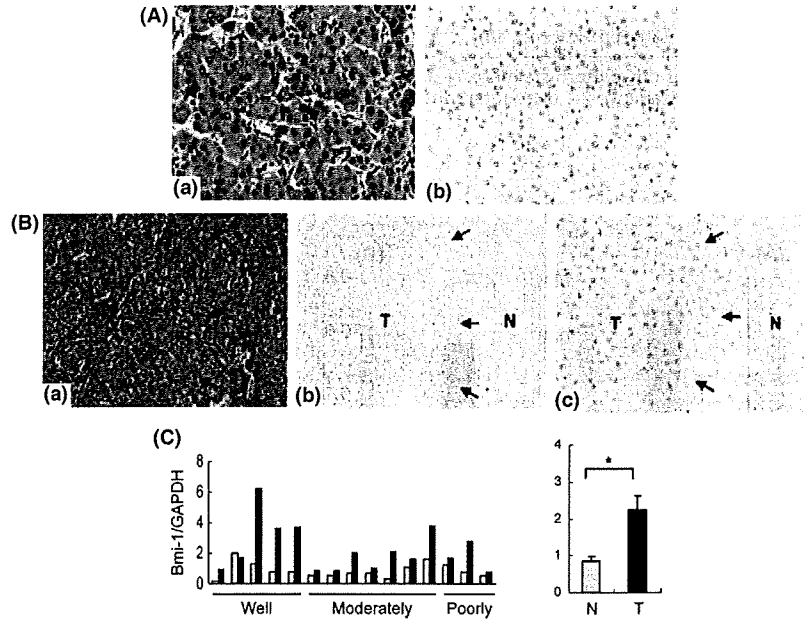

Fig. 2. *Bmi-1* expression in hepatocellular carcinoma (HCC) clinical samples. (A) Immunostaining of Bmi-1 in moderately differentiated HCC. Magnification, ×200. A clear dot-pattern of Bmi-1 was distributed diffusely in the tumor region. (B) Boundary region of well differentiated HCC (a, H&E stain; b, corresponding Bmi-1 staining, magnification ×100; c, magnification ×200). Bmi-1 expression was observed in the tumor region but not in surrounding liver tissue. Black arrows outline the border between the non-cancerous background region (N) and the tumor region (T). (C) *Bmi-1* mRNA expression levels in HCC clinical cases. The relative mRNA expression levels in tumor tissues (black bar, T) and corresponding non-cancerous, background liver tissues (gray bar, N) (left panel). High *Bmi-1* expression was observed in well differentiated HCC. The average expression level of *Bmi-1* was significantly higher in tumor tissues than in non-cancerous, background liver tissues (2.23 *vs* 0.86; *$P = 0.002$) (right panel).

Table 1. Characteristics of 122 hepatocellular carcinoma nodules on the basis of Bmi-1 immunostaining

Characteristics	Bmi-1 expression		*P* value
	2+/1+	–	
No. of nodules	101	21	0.339
Mean age (years)	62.7	60.2	NA
Gender			
Male	88	15	NA
Female	13	6	
Tumor size (cm)			
<2	37	6	0.482
≥2	64	15	
Differentiation			
Well (early)	35 (19)	2 (2)	0.023*
Moderately/poorly	66	19	
Portal involvement			
–	54	9	0.376
+	47	12	
Intrahepatic metastasis			
–	80	14	0.214
+	21	7	
Etiology			
Hepatitis B virus	21	7	NA
Hepatitis C virus	61	12	
Non-B / Non-C	19	2	
Non-cancerous liver			
Liver cirrhosis	51	10	0.810
Others	50	11	

*$P < 0.05$. –, absence of dot-pattern staining; 1+, distributed focally with weak dot-pattern staining; 2+, distributed diffusely with clear dot-pattern staining; NA, not available.

Table 2. Immunohistochemical analysis of Bmi-1 expression in hepatocellular carcinoma (HCC) (n = 122)

Histology	Bmi-1 staining score		
	2+	1+	–
Well differentiated HCC (n = 37)	24 (65%)	11 (30%)	2 (5%)
Early HCC (n = 21)	13 (62%)	6 (29%)	2 (10%)
Moderately differentiated HCC (n = 71)	32 (45%)	24 (34%)	15 (21%)
Poorly differentiated HCC (n = 14)	7 (50%)	3 (21%)	4 (29%)

–, absence of dot-pattern staining; 1+, distributed focally with weak dot-pattern staining; 2+, distributed diffusely with clear dot-pattern staining.

in 5 of 71 (7%) moderately differentiated HCCs, and in 3 of 14 (21%) poorly differentiated HCCs (Table 3). As expected, ABCB1 expression was also higher in the well differentiated HCCs. There was a correlation in ABCB1 and Bmi-1 staining (Fig. 4C), and 50 of 122 (41%) cases showed strong expression of both Bmi-1 and ABCB1 (Table 4).

Discussion

Following the identification of *Bmi-1* overexpression in solid tumors,[9,14–16] some studies have also reported the overexpression of *Bmi-1* in HCC.[17,18,23] However, the *Bmi-1* localization area and whether *Bmi-1* is highly expressed in the early or late progression of HCC is still controversial. In this study, high levels of *Bmi-1* expression were observed in early HCC, and we carefully describe the specific subcellular expression of *Bmi-1* within the nucleus. We believe that as a transcriptional repressor, *Bmi-1* activity is expected to occur inside the nucleus.[10,24,25] Moreover, we found a correlation in the expression of *Bmi-1* and *ABCB1* suggesting that *ABCB1* might present a novel downstream target for *Bmi-1*.

Bmi-1 belongs to the Polycomb gene group (PcG) involved in maintaining target genes in their transcriptional state. A possible mechanism of PcG-mediated repression is the recruitment of certain regulatory factors, or chromatin-modifying activities, into a unique nuclear domain which results in inhibiting chromatin remodeling required for the transcriptional process.[24] Indeed, there is evidence showing that 3D imaging of PcG proteins in Drosophila embryos shows distribution of PcG complexes throughout the nuclear volume as discrete loci, which might reflect sites of repressive complexes.[25] In accordance with previous reports, we observed that *Bmi-1* was expressed as high-intensity, small aggregates distributed inside the nucleus in the HCC region. The *Bmi-1* dots appeared in different parts of the nucleus, often very near to or partially coincident with heterochromatin. These findings support the indication of *Bmi-1* function as a gene transcriptional repressor by regulating chromatin silencing. Regarding this immunohistochemical staining dot-pattern as a positive expression of *Bmi-1*, we found high levels of *Bmi-1* expression in well (included early) differentiated HCCs, whereas similar expression was not observed in the corresponding non-cancerous background hepatocytes.

The *Bmi-1* signaling pathway is one of the candidates that might, in part, govern stem cell fate, and acquirement of its "stemness" function has been linked to neoplastic proliferation.[4,26] The ability of *Bmi-1* to promote tumorigenesis and bypass senescence through regulation of *p16* and hTERT expression[6–9] suggests a potential role of *Bmi-1* in initiating hepatocarcinogenesis and immortalization of the hepatocyte.

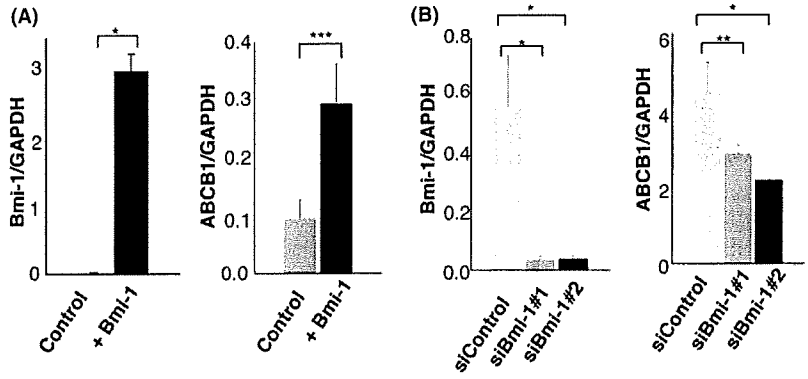

Fig. 3. Overexpression and silencing of *Bmi-1* expression affected ATP-binding cassette transporter B1 (*ABCB1*) expression in primary fetal hepatocytes and a hepatocellular carcinoma (HCC) cell line. (A) *Bmi-1* overexpression in primary fetal hepatocytes resulted in increased *ABCB1* expression, compared with the mock-transduced control (*$P < 0.01$; ***$P = 0.038$). (B) Silencing of *Bmi-1* expression by two different siRNAs (#1 and #2) in KIM-1 cells was followed by a decrease in *ABCB1* expression (*$P < 0.01$; **$P = 0.08$). Error bars were derived from three independent experiments.

doi: 10.1111/j.1349-7006.2009.01431.x

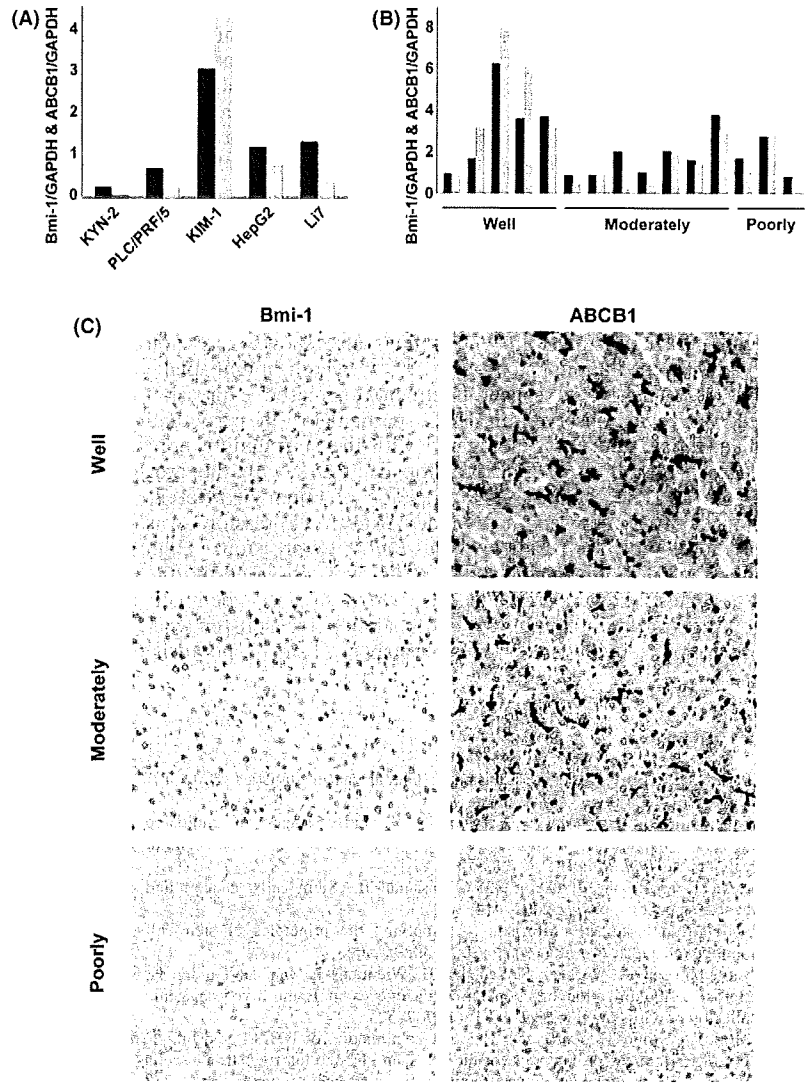

Fig. 4. Correlation and immunostaining of *Bmi-1* and ATP-binding cassette transporter B1 (*ABCB1*) expression in hepatocellular carcinoma (HCC). (A and B) Evaluation of *Bmi-1* and *ABCB1* mRNA expression in HCC cell lines and HCC clinical samples. A strong correlation between *Bmi-1* and *ABCB1* expression was observed in HCC cell lines and clinical samples by the Pearson's correlation coefficient test (0.95, $P = 0.01$; and 0.90, $P < 0.01$, respectively) (black column, *Bmi-1*; gray column, *ABCB1*). (c) Bmi-1 and ABCB1 expression in early, moderately, and poorly differentiated HCC (magnification, ×200). Clear staining of Bmi-1 "dot-pattern" (scored as 2+), and a canalicular and cytoplasmic ABCB1 staining pattern (scored as 2+), was observed in well differentiated HCC. Bmi-1 expression appeared weaker (scored as 1+), and only a canalicular staining pattern of ABCB1 (scored as 1+), was seen in moderately differentiated HCC. No dot-pattern of Bmi-1 and an absence of ABCB1 staining were observed in poorly differentiated HCC (scored as negative). Both Bmi-1 and ABCB1 expression decreased with the progression of HCC, suggesting their correlated expression.

Table 3. Immunohistochemical analysis of ATP-binding cassette transporter B1 (ABCB1) expression in hepatocellular carcinoma (HCC) (n = 122)

Histology	ABCB1 staining score		
	2+	1+	–
Well differentiated HCC (n = 37)	29 (78%)	7 (19%)	1 (3%)
Early HCC (n = 21)	18 (86%)	3 (14%)	0 (0%)
Moderately differentiated HCC (n = 71)	50 (70%)	16 (23%)	5 (7%)
Poorly differentiated HCC (n = 14)	10 (71%)	1 (7%)	3 (21%)

–, no staining; 1+, irregular canalicular staining pattern; 2+, clear staining of irregular canalicular with cytoplasmic staining.

Table 4. Combined immunohistochemical analysis of *Bmi-1* and ATP-binding cassette transporter B1 (ABCB1) expression in hepatocellular carcinoma

ABCB1 staining score Bmi-1 staining score	2+	1+	–
2+	50 (41%)	12 (10%)	1 (1%)
1+	28 (23%)	7 (6%)	3 (2%)
–	11 (9%)	5 (4%)	5 (4%)

ABCB1 staining scores: –, no staining; 1+, irregular canalicular staining pattern; 2+, clear staining of irregular canalicular with cytoplasmic staining. Bmi-1 staining scores: –, absence of dot-pattern staining; 1+, distributed focally with weak dot-pattern staining; 2+, distributed diffusely with clear dot-pattern staining.

Low levels of *p16* expression and increased activation of hTERT have also been reported in HCC, including in early HCC.[19,27,28] We observed high levels of *Bmi-1* expression in early HCC, which might indicate an indispensable function for *Bmi-1* in the early development of cancer. *Bmi-1* expression was also observed in progressed HCC, however, the expression level was not as high as in early HCC. This findings suggested *de novo* tumor development pathways as well as indicated another functional role of *Bmi-1* in progressed HCC. Although it is clear that *Bmi-1* plays a role in keeping self-renewal ability and proliferation, the exact molecular mechanism of *Bmi-1* in early hepatocarcinogenesis remains unclear. Inactivation of *p16* expression by methylation or epigenetic mechanisms has already been observed as an early